AD-A203 427

DTIC FILE COPY

(2)

UNCLASSIFIED

SECURITY CLASSIFICATION OF THIS PAGE (When Data Entered)

REPORT DOCUMENTATION PAGE		READ INSTRUCTIONS BEFORE COMPLETING FORM
1. REPORT NUMBER ARO 22773.2-GS	2. GOVT ACCESSION NO. N/A	3. RECIPIENT'S CATALOG NUMBER N/A
4. TITLE (and Subtitle) The Development and Structure of Nocturnal Slope Winds in a Simple Valley Final Report		5. TYPE OF REPORT & PERIOD COVERED Final Report September 1985-December 1988 6. PERFORMING ORG. REPORT NUMBER
7. AUTHOR(s) J.C. Doran T.W. Horst C.D. Whiteman		8. CONTRACT OR GRANT NUMBER(s) DAAG29-85-K-0231
9. PERFORMING ORGANIZATION NAME AND ADDRESS Battelle, Pacific Northwest Laboratories P.O. Box 999, Richland, WA 99352		10. PROGRAM ELEMENT, PROJECT, TASK AREA & WORK UNIT NUMBERS N/A
11. CONTROLLING OFFICE NAME AND ADDRESS U. S. Army Research Office Post Office Box 12211 Research Triangle Park, NC 27709		12. REPORT DATE December 1988 13. NUMBER OF PAGES 96
14. MONITORING AGENCY NAME & ADDRESS(if different from Controlling Office)		15. SECURITY CLASS. (of this report) Unclassified 15a. DECLASSIFICATION/DOWNGRADING SCHEDULE

16. DISTRIBUTION STATEMENT (of this Report)

Approved for public release; distribution unlimited.

DTIC ELECTE JAN 23 1989 S D CSD

17. DISTRIBUTION STATEMENT (of the abstract entered in Block 20, if different from Report)

NA

18. SUPPLEMENTARY NOTES

The view, opinions, and/or findings contained in this report are those of the author(s) and should not be construed as an official Department of the Army position, policy, or decision, unless so designated by other documentation.

19. KEY WORDS (Continue on reverse side if necessary and identify by block number)

Slope flows
Drainage flows
Complex terrain meteorology
Valley temperature inversions
Thermally-developed wind systems

20. ABSTRACT (Continue on reverse side if necessary and identify by block number)

This report describes the results of a project to study the evolution and structure of nocturnal slope flows that form on the sidewalls of a simple valley. The valley chosen for the project was located in southeastern Washington. The measurement sites were located in a straight 1.5 km long section of the valley, with the ridgetops approximately 225 m above the valley floor. The east sidewall was quite smooth, had little vegetation other than grasses, and had a nearly constant 23 degree slope angle. The west sidewall was more irregular, steeper, and had more vegetation. Towers were erected on both sidewalls, and wind and temperature data were collected there on six nights in October of 1986. A Doppler sodar measured winds

DD FORM 1 JAN 73 1473 EDITION OF 1 NOV 65 IS OBSOLETE

UNCLASSIFIED

SECURITY CLASSIFICATION OF THIS PAGE (When Data Entered)

89 1 17 310

20. ABSTRACT CONTINUED

throughout the depth of the valley and above, and a tethered balloon was used to obtain temperature measurements and additional wind data in the valley during the first few hours after sunset.

Cooling in the valley began with the rapid development of a strong inversion near the valley floor. At approximately 1830 PDT this inversion began to mix rapidly through the depth of the valley, and the winds in the valley changed from a shallow layer of down-valley flow under a deeper layer of up-valley flow to down-valley flow over the whole depth of the valley. During this time the temperature profile in the valley often developed one or more layers of constant potential temperature some tens of meters deep. Down-valley wind speeds increased and typically reached 6 to 7 m/s at a height of about 75 m. By approximately 2200 PDT winds were sufficiently strong and gusty so that further temperature soundings with a tethered balloon were no longer possible.

Most of the analyses of slope flows concentrated on the east sidewall because of its smoother topography. Three towers, designated A, B, and C were located along the fall line of the slope at nominal heights of 150, 100, and 50 m above the valley floor, respectively. The inversions on this sidewall were described well in terms of two parameters, an inversion strength ΔT and an e-folding inversion depth, h. The inversion depths were found to be roughly twice as large at tower A as at B and C, with a maximum value at A of about 3 m shortly after local sunset, decreasing to approximately 2 m later in the night. The inversion strengths at towers A and B were in general quite similar to each other and about 50% grater than at tower C. The inversion strengths at towers A and B had maximum values on the order of 4 K and 3.5 K, respectively, just after local sunset, but decreased to about 1.2 K for most of the night. The inversion strength at C had a smaller peak of about 1.4 K, and a value of approximately 0.8 K for a steady state value.

The inversion strengths at the towers appear to be affected strongly by the down-valley winds. Inversion strengths greater than 2 K at towers A and B occurred only for along-valley wind speeds of less than 4 m/s; at higher speeds turbulent mixing reduced the values of ΔT. For comparable wind speeds at the three towers, the generally stronger ambient stratification at the level of tower C further reduced the inversion strength.

Although there was clear evidence of a local maximum in the downslope wind component, the position and strength could not be resolved with only three anemometers at each tower. Consequently, useful scaling parameters to characterize the structure of the katabatic winds were not found. Evidence for katabatic winds was found at heights of 6 m, but possible contributions from ambient cross-valley flows complicated the interpretation of the data. The low-level downslope wind speeds (~1.5 m height) were shown to be sensitive to the magnitude of the local buoyancy deficit, which is proportional to the product $h \cdot \Delta T$, but only for weak along-valley winds. For along-valley wind speeds greater than 2 m/s, the downslope winds showed little sensitivity to the strength of the buoyancy deficit. Typical downslope wind speed values ranged between 0.5 and 1.0 m/s.

Significant cross-valley temperature gradients were found. These precluded using the valley temperatures as a good quantitative predictor of the slope flow characteristics. However, the presence of adiabatic regions in the potential temperature structure appears to be associated with decreases in the sidewall inversion depth. This result was supported by numerical simulations, which also emphasized the distinction between depth scales characterizing the inversion, h, and the mass or momentum transport, h'. The two quantities behave similarly over simple slopes, i.e., those not part of a valley system. However, in a valley where the ambient stratification changes significantly with height, the two quantities develop quite differently as a function of downslope distance. Observations and model results also showed that assumptions of constant sensible heat fluxes or temperature differerences between the ambient atmosphere and the sidewalls, previously used in some models, may be inappropriate.

ARO 22773.2-GS

THE DEVELOPMENT AND STRUCTURE OF NOCTURNAL SLOPE WINDS IN A SIMPLE VALLEY

Final Report

J. C. Doran
T. W. Horst
C. D. Whiteman

December 1988

Prepared for
Army Research Office
Research Triangle Park, NC 27709
under Contract DAAG29-K-0231

Battelle
Pacific Northwest Laboratories
Richland, Washington 99352

Approved for Public Release;
Distribution Unlimited

ACKNOWLEDGMENTS

This research was supported by the U.S. Army Research Office under contract number DAAG29-K-0231. Additional support to deploy the Doppler sodar and reduce the sodar data was provided by the U.S. Department of Energy under contract DE-AC06-76RLO 1830. Mr. W.C. Pulliam, Mr. D. Rainwater, and Mr. W. Carlton, Jr. are thanked for permission to use their land and for their cooperation during the course of the field measurement program. O. B. Abbey, G. W. Dennis, J. M. Hubbe, J. Buck, M. Schmeeckle, and D. Dovey assisted in setting up and maintaining the field equipment. J. M. Hubbe also assisted in data processing.

CONTENTS

FIGURES

TABLES

SUMMARY

This report describes the results of a project to study the evolution and structure of nocturnal slope flows that form on the sidewalls of a simple valley. The valley chosen for the project was located in southeastern Washington. The measurement sites were located in a straight 1.5-km-long section of the valley, with the ridgetops approximately 225 m above the valley floor. The east sidewall was quite smooth, had little vegetation other than grasses, and had a nearly constant 23-degree slope angle. The west sidewall was more irregular, steeper, and had more vegetation. Towers were erected on both sidewalls, and wind and temperature data were collected there on six nights in October of 1986. A Doppler sodar measured winds throughout the depth of the valley and above, and a tethered balloon was used to obtain temperature measurements and additional wind data in the valley during the first few hours after sunset.

Cooling in the valley began with the rapid development of a strong inversion near the valley floor. At approximately 1830 PDT, this inversion began to mix rapidly through the depth of the valley, and the winds in the valley changed from a shallow layer of down-valley flow under a deeper layer of up-valley flow to down-valley flow over the whole depth of the valley. During this time, the temperature profile in the valley often developed one or more layers of constant potential temperature some tens of meters deep. Down-valley wind speeds increased and typically reached 6 to 7 m/s at a height of about 75 m. By approximately 2200 PDT, winds were sufficiently strong and gusty so that further temperature soundings with a tethered balloon were no longer possible.

Most of the analyses of slope flows concentrated on the east sidewall because of its smoother topography. Three towers, designated A, B, and C, were located along the fall line of the slope at nominal heights of 150, 100, and 50 m above the valley floor, respectively. The inversions on this sidewall were described well in terms of

two parameters, an inversion strength, ΔT, and an e-folding inversion depth, h. The inversion depths were found to be roughly twice as large at tower A as at B and C, with a maximum value at A of about 3 m shortly after local sunset, decreasing to approximately 2 m later in the night. The inversion strengths at towers A and B were in general quite similar to each other and about 50% greater than at tower C. The inversion strengths at towers A and B had maximum values on the order of 4 K and 3.5 K, respectively, just after local sunset, but decreased to about 1.2 K for most of the night. The inversion strength at C had a smaller peak of about 1.4 K, and a value of approximately 0.8 K for a steady-state value.

The inversion strengths at the towers appear to be affected strongly by the down-valley winds. Inversion strengths greater than 2 K at towers A and B occurred only for along-valley wind speeds of less than 4 m/s; at higher speeds, turbulent mixing reduced the values of ΔT. For comparable wind speeds at the three towers, the generally stronger ambient stratification at the level of tower C further reduced the inversion strength.

Although there was clear evidence of a local maximum in the downslope wind component, its position and strength could not be resolved with only three anemometers at each tower. Consequently, useful scaling parameters to characterize the structure of the katabatic winds were not found. Evidence for katabatic winds was found at heights of 6 m, but possible contributions from ambient cross-valley flows complicated the interpretation of the data. The low-level downslope wind speeds (~1.5-m height) were shown to be sensitive to the magnitude of the local buoyancy deficit, which is proportional to the product $h \cdot \Delta T$, but only for weak along-valley winds. For along-valley wind speeds greater than 2 m/s, the downslope winds showed little sensitivity to the strength of the buoyancy deficit. Typical downslope wind speed values ranged between 0.5 and 1.0 m/s. Significant cross-valley temperature gradients were found. These precluded using the valley temperatures as a good quantitative predictor of the slope flow characteristics.

However, the presence of adiabatic regions in the potential temperature structure appears to be associated with decreases in the sidewall inversion depth. This result was supported by numerical simulations, which also emphasized the distinction between depth scales characterizing the inversion, h, and the mass or momentum transport, h'. The two quantities behave similarly over simple slopes, i.e., those not part of a valley system. However, in a valley where the ambient stratification changes significantly with height, the two quantities develop quite differently as a function of downslope distance. Observations and model results also showed that assumptions of constant sensible heat fluxes or temperature differences between the ambient atmosphere and the sidewalls, previously used in some models, may be inappropriate.

INTRODUCTION

The work described in this report is part of a systematic study for the Army Research Office (ARO) of the influence of terrain on the wind and temperature fields in the nocturnal boundary layer. While there have been numerous programs that have addressed this problem, most have concentrated on larger scale terrain features such as deep mountain valleys. To complement these studies and to limit the complexity of the problem, this ARO program has concentrated on scales that include terrain features less than a few hundred meters in vertical extent and horizontal distances on the order of a few kilometers or less. An earlier project focused on the turbulent structure of nocturnal drainage flows that form over a simple slope (i.e., a two-dimensional slope on the side of an isolated mountain or ridge). Measurements were taken over a section of Rattlesnake Mountain, near Richland, Washington, and the results were analyzed in terms of local similarity theory. Combined with related work for the U.S. Department of Energy's Atmospheric Studies in Complex Terrain (ASCOT) program, that study provided considerable understanding of the characteristics of these flows in simple terrain. The area of study was a nearly two-dimensional slope, and the ambient conditions in which the slope flows developed were relatively free from strong cross-slope winds, strong stratification or stratification that changed rapidly with height, terrain-induced channeling, or other problems associated with more complex topography. However, such slopes are more the exception than the rule, and it was recognized that the work would have to be extended to take into account factors such as these.

The next step was to extend these studies to the sloping sidewalls of a simple valley. In particular, we wished to compare and contrast the development and structure of katabatic flows over a valley sidewall to that found over a simple slope. Because of this desire to concentrate on the effects of the valley environment without introducing a host of other complicating factors, a simple valley had to satisfy a number of criteria. The valley had to be long enough so that down-valley drainage winds would

develop reliably on clear nights. The valley sidewalls should be quite uniform in slope and not too steep. Any vegetation on the slopes should be rather sparse to avoid complications from canopy effects on the wind and temperature fields. For ease of obtaining vertical profiles of wind and temperature, the valley should not be too deep, and ready access to the valley floor and sidewalls was also required. Tributaries should not be a major topographical feature, and the section of the valley chosen for study must be rather straight. Finally, for logistical reasons, the valley had to be located within a few hours' drive from our laboratory in Richland, Washington. In practice, some compromises were likely to be necessary. A description of the site actually chosen for our study is given in the next section.

Before the measurement phase of this project, a simple conceptual picture was developed for some of the features of slope flows expected in a simple valley. Katabatic winds form over a slope in response to the temperature difference between the cooled air in the vicinity of the slope and the warmer air found at the same elevation but farther from the slope. As a local inversion forms over a valley sidewall, a downslope wind will develop there. However, an inversion also forms over the valley floor, and as this inversion deepens, more of the sidewalls will be contained within this cold layer. The local inversions on the sidewalls should then weaken in these regions, so that the katabatic winds should also become weaker. Moreover, as the along-valley winds increase, the winds on the slopes were expected to turn more toward the down-valley direction.

Some of these features were, in fact, observed and will be described in later sections. However, the behavior was not always consistent with this simple picture, and modifications in our original description were required. We also hoped to be able to describe the dependence of the slope wind and temperature structure on the ambient valley conditions in terms of a few simple parameters related to the valley winds and the temperature differences between the valley center and the sidewalls. Although the actual behavior proved to be too complicated for such a simple

parametric scheme, it was possible to provide some useful descriptions of the slope flow characteristics and to relate these to features of the ambient valley meteorology.

This report begins with a description of the field site and the layout of the various instruments that were deployed. A brief summary of the synoptic conditions during the measurement period is then provided. This is followed by a description of the structure and evolution of wind and temperature fields in the valley. These features of the valley meteorology are important because they constitute the ambient conditions under which the slope flows develop, and they play a major role in determining slope flow behavior. The next section then discusses the structure of the katabatic winds on the valley sidewalls. The discussion includes descriptions of the strengths and depths of the inversions that form over the slopes and descriptions of some of the characteristics of the katabatic winds. It also describes the time-varying behavior of these features and their relationship to the changing ambient conditions. The similarities and differences in the behavior of slope flows over simple slopes and over valley sidewalls are also summarized. A numerical model was used to study further some features of the slope winds, and these studies are described in the following section. Numerical simulations are used to illustrate the critical role played by the structure of the valley inversion in determining the downslope evolution of the slope flows. They also clarify the difference between inversion and momentum length scales and how these scales are related to each other over simple slopes and over valley sidewalls. The last section contains conclusions from the study and suggests areas of future research that would allow one to more fully describe the influence of terrain on the wind and temperature fields in the first few hundred meters above the surface. Two appendices contain additional information that may be of interest. Appendix A describes some features of the atmospheric and surface energy budgets in the valley, while Appendix B provides some details about the model used for the numerical simulations.

SITE DESCRIPTION AND INSTRUMENTATION

SITE DESCRIPTION AND INSTRUMENT DEPLOYMENT

The experimental period extended for approximately 4 weeks, from early September to October 10, 1986. The initial testing period for the instruments, data loggers, and procedures was followed by a prolonged period of unsettled weather. Conditions began to improve on the evening of October 3, and during the following six nights (October 4-5 through October 9-10) the weather was quite favorable, with clear skies, generally weak winds aloft, and consistent down-valley winds forming after sunset. For convenience, these periods are referred to as Julian days (JD) 276-277 through 282-283, and the Julian dates and calendar dates will be used interchangeably in this report. Table 1 lists the conversions between the two sets of dates.

TABLE 1. Conversion Between Calendar Date and Julian Date

Date, 1986	Julian Day
3 October	276
4 October	277
5 October	278
6 October	279
7 October	280
8 October	281
9 October	282

A valley in southeastern Washington was selected for our study site. The valley lies near the town of Dayton and was formed by the South Fork of the Touchet River as it flows out of the Blue Mountains. Figure 1 shows a topographical map of the area, and Figure 2 shows an enlarged section of the map for the area where the measurements were taken. In this area, the valley is approximately 225 m deep, and

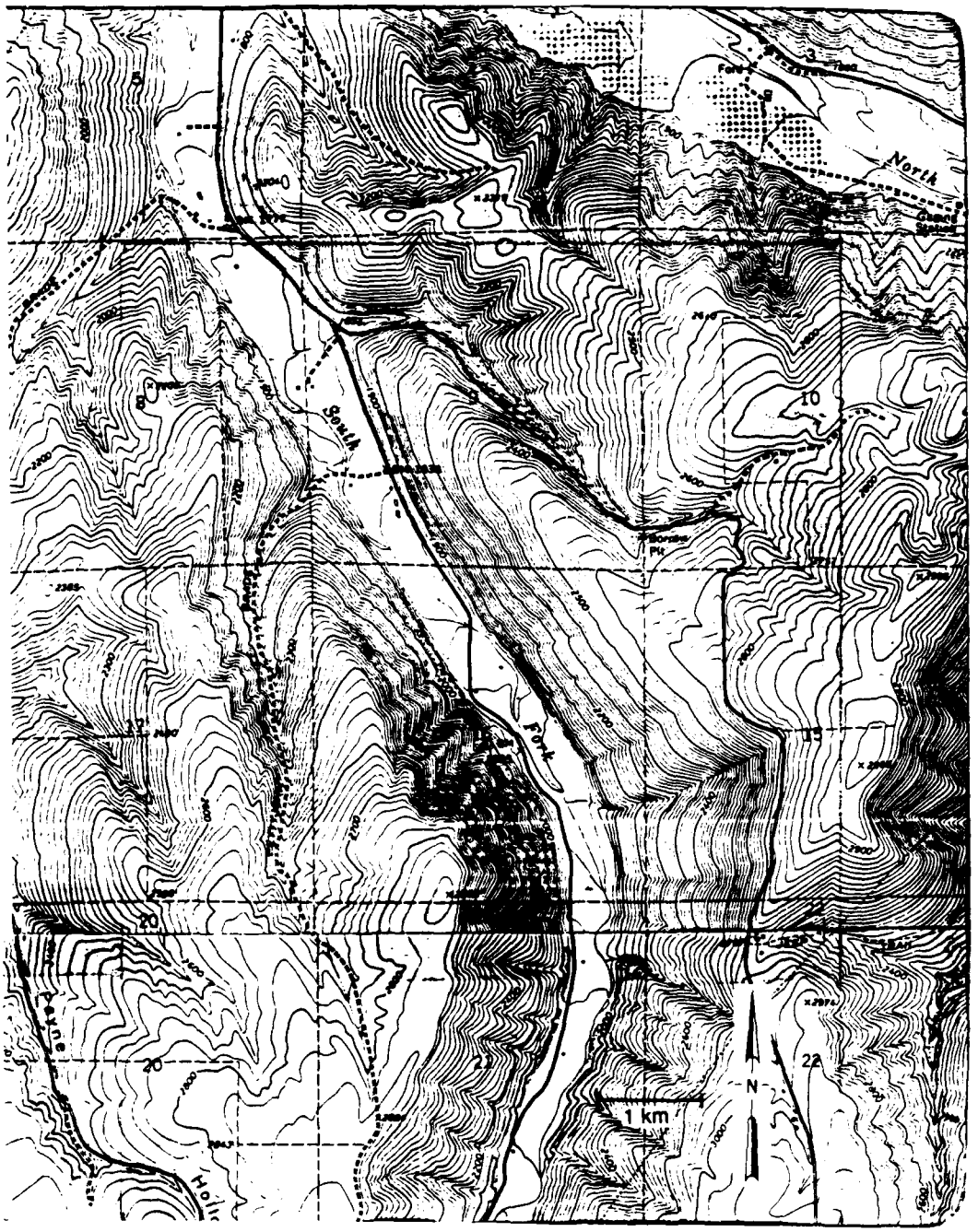

FIGURE 1. Topographical Map of South Fork of Touchet River. Measurements sites lie near center of figure. Contour heights in feet.

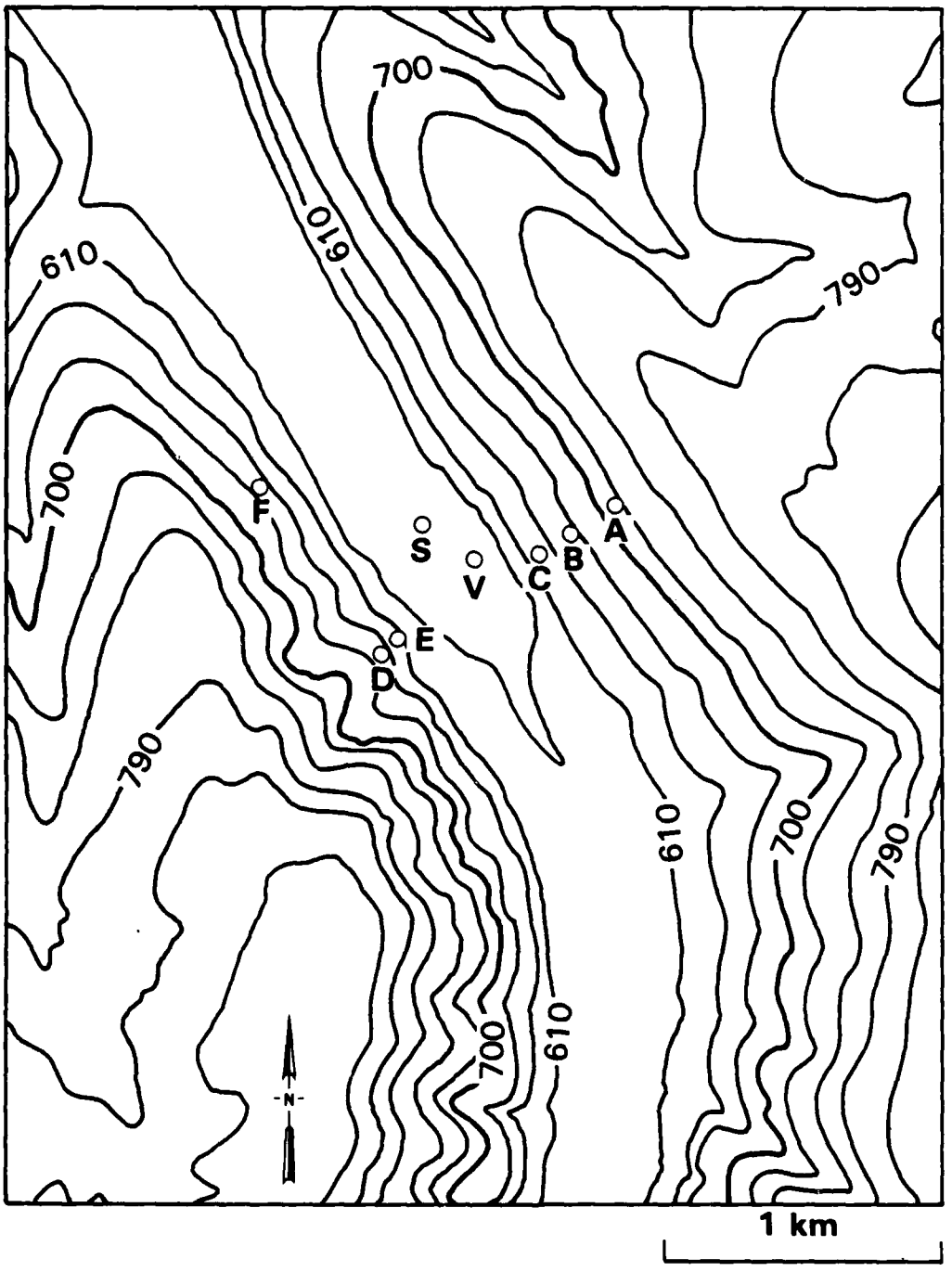

FIGURE 2. Topographical Map of Measurement Sites. Locations of Towers A through F are shown. S: sodar; V: 61-m tower, contour heights in meters.

runs from southeast to northwest. The east sidewall in our study area has a section of particularly uniform slope angle that extends for about 1.5 km along the valley and over most of the vertical extent from the ridgeline to the valley floor. The slope angle in this area is about 23 degrees, except for the lowest portions of the slope where the angle increases to about 40 degrees. Vegetation consists primarily of dry grasses; trees near the river on the valley floor do not extend up the sidewall. Figure 3 shows a photograph of this section of the valley.

Three 9-m towers were located on this sidewall at the positions labeled A, B, and C in Figure 2. The base elevations of the towers were nominally 50, 100, and 150 m above the valley floor, and were all located on the section of the slope with a nearly constant slope angle. Thermocouples measured the temperature at six levels on each of the towers, and three-component propeller anemometers measured the wind velocity at three levels. Net radiation was also recorded at each of the towers. All data were sampled at 2-s intervals, averaged for periods of 2 min, and written to cassette tapes. (For displaying time series in many of the figures to be shown, the data were smoothed further, using approximately 10% of the data for smoothing at each point.) Table 2 lists the instrument heights at each of the towers. The highest anemometer at tower A was located at a lower height than the corresponding instruments at towers B and C because measurements over simple slopes suggested that the katabatic layer would be shallower at tower A than at B or C.

Three additional 9-m towers were placed on the west sidewall. The west sidewall is considerably more convoluted, and portions of it are covered with low bushes and some trees. Directly opposite the smooth section of the east sidewall was a roughly triangular section of slope, with an apex 100 m above the valley floor and was bounded by gullies on the up-valley and down-valley sides. The slope angle over this section is between 32 and 35 degrees. Tower D was located near the top of this feature, at about the same elevation as tower B, but here only temperatures were recorded. A path-averaging anemometer measured the up- and down-valley wind components on a path between towers B and D. Tower E was located at

FIGURE 3. Photograph of East Sidewall and Valley Floor. Sodar cones are visible in the left foreground, and the 61-m tower is to the right of the instrument trailer.

approximately the same height as tower C, and had similar instrumentation. A somewhat smoother and more uniform section of slope, with an angle of about 28 degrees, was found about half a kilometer farther down-valley. Tower F was placed here, again at approximately the same height as tower B and with similar instrumentation. Instrument heights for the west sidewall towers are also given in Table 2.

TABLE 2. Heights of Temperature (T) and Wind (W) Sensors on Sidewall and Valley Towers. All heights are in meters. Number in parentheses below tower is elevation of tower base above valley floor in meters.

Tower A	T:	0.18, 0.61, 1.35, 2.82, 5.74, 8.99
(147)	W:	0.66, 1.47, 3.51
Tower B	T:	0.13, 0.56, 1.35, 2.79, 5.87, 8.94
(99)	W:	0.74, 1.46, 6.00
Tower C	T:	0.18, 0.58, 1.35, 2.85, 5.89, 8.94
(52)	W:	0.63, 1.47, 5.89
Tower D	T:	0.11, 0.48, 1.40, 2.90, 5.94, 8.61
(92)		
Tower E	T:	0.11, 0.45, 1.21, 2.73, 5.73, 8.67
(52)	W:	1.52, 3.09, 5.92
Tower F	T:	0.11, 0.58, 1.35, 2.95, 5.99, 8.89
(88)	W:	0.74, 1.35, 5.99
Valley Tower	T	7.62,17.1,32.3,47.5, 62.4
	W:	3.05, 7.62, 17.4, 32.7, 47.9, 63.1

Because the east sidewall is much more regular in its slope angle and because its vegetation is much simpler, most of our efforts have been concentrated on the analysis of the data collected from towers A, B, and C, rather than D, E, and F.

However, differences and similarities in the slope flows on the two sides of the valley will be described at a number of places in this report.

On the valley floor, a 61-m tower was erected to record wind and temperature profiles at the lower levels of the valley. The tower had six levels of three-component propeller anemometers for wind measurement and five levels of thermistors for temperature measurement. Instrument heights for the valley floor tower are listed in Table 2 as well.

A three-component Doppler sodar was used to record the winds over the depth of the valley and above. Doppler wind data were collected over 25-m range gates and averaged over 10-min time intervals.

During the evening transition periods, an instrument package was flown on a tethered balloon (Tethersonde®, Atmospheric Instrumentation Research, Inc., Boulder, Colorado) to record the temperature structure in the center of the valley and above the ridge tops. The tethered balloon data collection system also provided wind speed and direction information to supplement that obtained from the sodar and path-averaging anemometers. Balloon flights were made approximately every 20 to 30 min from about 1630 to 2100 PDT.

INSTRUMENT CALIBRATION AND DATA RECOVERY

Thermistors and thermocouples were calibrated in a temperature-controlled bath against NBS-traceable, calibrated mercury-in-glass thermometers. The accuracy obtained in the field for the thermocouple sensors depends in large part on the degree to which a metal strip in the data logger, used to provide a reference temperature, is free from temperature gradients. There was no way of determining gradients, but to minimize possible temperature inhomogeneities, the data loggers on all the sidewall towers were enclosed in insulated picnic coolers. These shielded the loggers from sudden temperature changes caused by advective or radiative

effects; the resultant accuracy of the tower measurements is estimated to be approximately 0.2 K or better.

The propeller anemometers were calibrated by driving the miniature generators in the shafts with a constant rpm motor and adjusting the voltage output to a known value. This was done for each arm of each anemometer. Speeds obtained from the anemometers were estimated to be accurate to about 5 cm/s or better.

The 61-m tower data of most interest are the wind and temperature data at the top of the tower, because the top of tower C and the top of the 61-m tower are nearly at the same height. The calibration of the 61-m tower thermistors suggested that they were accurate to 0.2 K or better. Temperatures measured at the top of the tower were also compared with the temperatures recorded by the tethered balloon system (which also used a thermistor for its sensor) as it drifted slowly past the top of the tower during its ascents. The time constant of the sensor on the balloon package was sufficiently short (~ 12 s) and the ascent rate sufficiently slow (~ 0.5 m/s) that such comparisons should agree within a few tenths of a degree or better. Data averaged from 57 balloon soundings showed the tower averaging about 0.3 K cooler than the balloon-borne sensor. However, when the top of the tower was in sunlight, the tower temperature was somewhat warmer than the sonde temperature, while it was cooler when the top of the tower was in shadow. This suggests that the aspiration of the tower thermistors may not have been as effective as was wished. This discrepancy should have little or no effect on the analyses to be discussed because most of our analyses do not involve temperature differences between the valley center and the valley sidewalls. For those that do, a temperature offset of a few tenths of a degree would not significantly alter any conclusions that were reached.

Data recovery was generally good. Some problems were experienced with the logger at tower C, particularly on the night of JD 280-281. There were also failures in the logger operation at the main tower late in the evening of JD 278 and several hours before sunrise on the morning of JD 282. During the evening transition period,

when the up- and down-valley winds were usually quite weak, data recovery from the sodar was intermittent at some levels because of poor echoes. After 2000-2100 PDT, rather strong and gusty winds were found in the first 100 meters above the surface, and these winds prevented us from flying the tethered balloon. The winds made the balloon bounce violently, and blew it in the direction of a prominent line of trees down-valley from our launch site. Thus, temperature soundings are not available after these times.

AMBIENT METEOROLOGY

SYNOPTIC METEOROLOGY

During the 3-10 October period, synoptic weather patterns produced rather uniform flows and temperatures over the Dayton experimental area. A weak blocking pattern persisted during the entire period off the Pacific Coast. A high pressure cell remained stationary offshore of Washington and Oregon with a weak low pressure center near the southern California Coast. Flow onto the West Coast of the United States was forced by this pressure pattern to deviate north of the high pressure center and come onshore in British Columbia before turning south to flow around the ridge aloft. The experimental area was thus under the influence of a high pressure center, which produced generally northerly or northwesterly winds over the experimental area during the entire period. Surface winds were generally light, but winds aloft were accelerated around the ridge by low pressure centers in the interior of the continent, so that the northwesterly winds increased in strength with altitude.

Rawinsonde soundings at Spokane, Washington, and Salem, Oregon (Figure 4 for locations), illustrate the resulting synoptic wind variations during the experimental period (Figures 5 and 6). Figure 7 shows the resulting temperature variations at standard pressure levels from the Spokane sounding. Temperatures rose slowly during the 3-6 October period, and then fell during the 6-10 October period.

The reader is referred to the wind arrows on Figure 5 plotted between the surface and 850 hPa winds. These wind arrows represent above-valley (275 m AGL) Doppler winds observed at 0200 PDT. These winds have a southerly component and, clearly, bear no relationship to the synoptic winds at Spokane or Salem. The valley orientation is such that a down-valley wind blows from the southeast (i.e., from ~150 degrees). The Doppler sounder shows that above-valley winds on the different nights generally have a down-valley component but also have

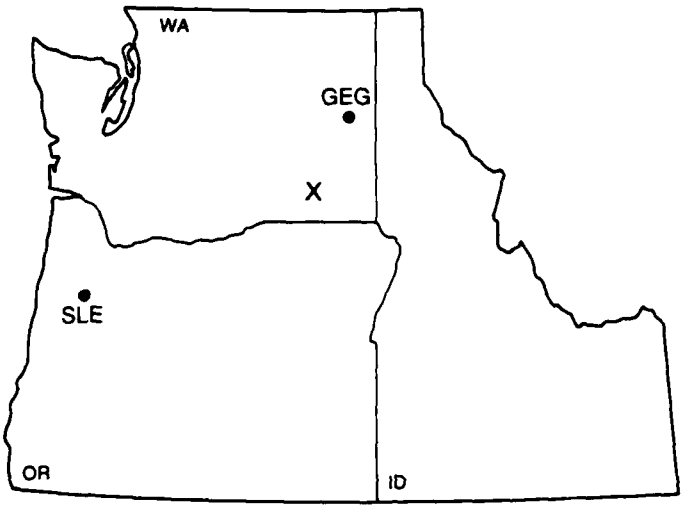

FIGURE 4. Location of Experimental Site (X) Relative to National Weather Service Rawinsonde Stations (GEG = Spokane; SLE = Salem)

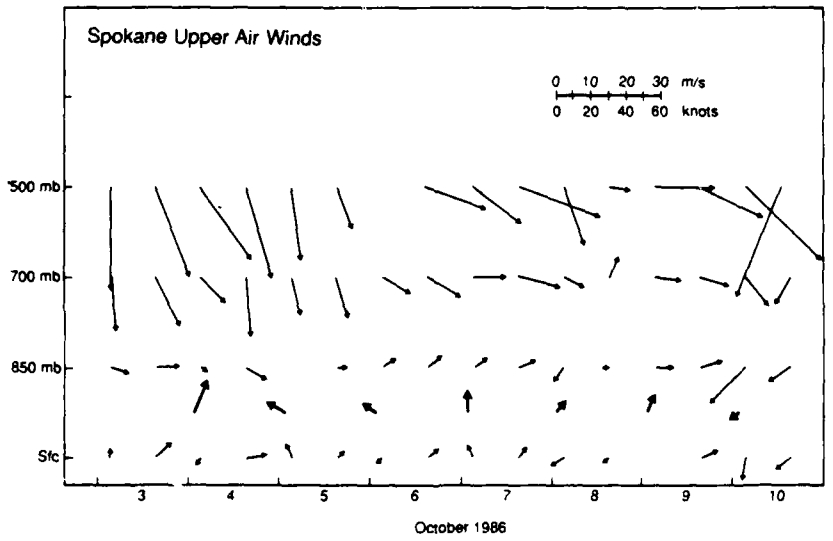

FIGURE 5. Rawinsonde-Observed Winds at Spokane, Washington, 3-10 October 1986. Bold arrows are Touchet Valley Doppler winds at 275 m AGL.

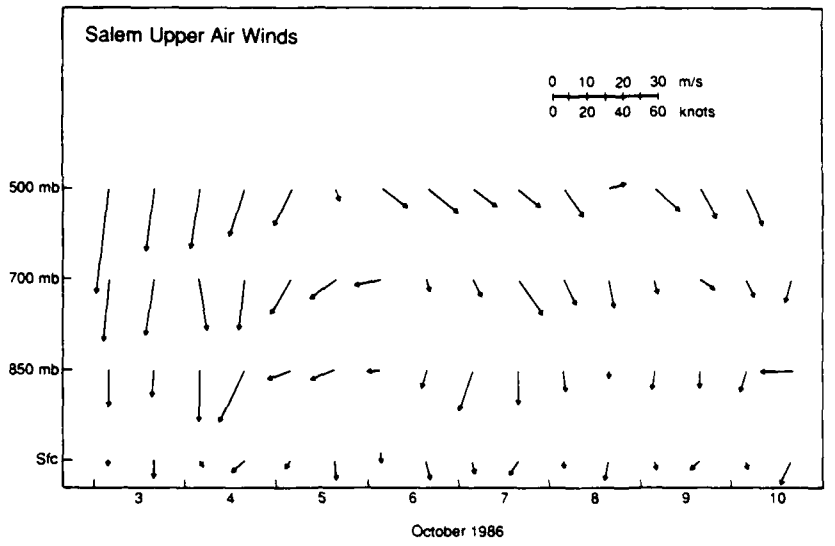

FIGURE 6. Rawinsonde-Observed Winds at Salem, Oregon, 3-10 October 1986.

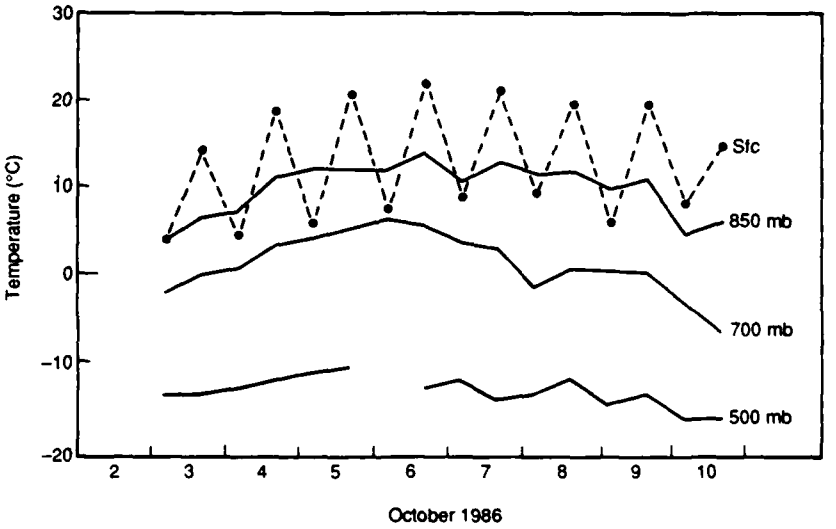

FIGURE 7. Rawinsonde-Observed Temperatures at Spokane, Washington, for Standard Pressure Levels, 4-11 October 1986.

appreciable cross-valley components - sometimes from one side of the valley and sometimes from the other.

Above-valley winds are thus apparently forced by mesoscale circulations that are not resolved by the synoptic scale rawinsonde network. Because the above-valley Doppler-observed winds are southerly, they are likely to represent a mesoscale drainage flow from the Blue Mountains south of the observation site. The southerly component at 275 m is thus not merely the upward extension of the nighttime down-valley flow observed within the valley, but represents a larger scale flow. This conclusion is supported by the Doppler data and the Tethersonde® data that extended higher than the 275-m level. The flow may be channeled by sections of the valley farther upstream where the ridge lines are higher.

The reason for the varying sign of the cross-valley wind component from night to night is unknown at present, and sufficient data to resolve mesoscale questions such as this were not collected as part of the experimental design. Nevertheless, the Doppler sodar is clearly able to observe the mesoscale wind field above the valley and its variation in time, so that the slope wind experiments can be placed within a broader mesoscale flow context.

VALLEY METEOROLOGY

Evolution of Valley Temperature and Wind Structure on JD 277-278

Sequential Tethersonde® profiles taken from the valley center showed similar temperature and wind structure evolution from night to night. Analyses have emphasized the nights of JD 277, JD 278, and JD 281. On these nights the down-valley winds and the downslope winds on the sidewalls were particularly steady for most of the night. In this section temperature and wind structure evolution during the evening transition period are illustrated by focusing on two of these nights, JD 277 and JD 278.

In Figure 8, the first potential temperature sounding of the JD 277 sequence, at 1545 PDT, found a shallow superadiabatic layer present near the ground surmounted by a well-mixed, nearly-constant potential temperature atmosphere. The constant potential temperature layer contained up-valley winds with speeds of 1 to 2 m/s (Figure 9). Subsequent temperature soundings, taken at roughly 30-min intervals, showed rapid cooling in a growing stable boundary layer above the valley floor. The cooling was confined initially to this near-ground layer, with the inversion attaining strengths of 6 or 7 K through depths of less than 100 m. Winds within the growing inversion layer reversed to down-valley, while the winds in the upper levels of the valley maintained their up-valley direction. The character of the temperature structure evolution changed abruptly between the 1818 and the 1845 PDT soundings, at a time when the winds in the upper part of the valley atmosphere suddenly reversed to down-valley. This change in character was a typical feature of the meteorology of this valley during the experimental period. Specifically, the initial shallow, but intense, near-ground temperature deficit (i.e., inversion) became mixed through the entire valley depth so that the upper levels of the valley atmosphere began to cool at a faster rate than the surface layers. Eventually, over the next 1 to 2 hours the mixing associated with the strengthening down-valley winds distributed the cooling through the valley atmosphere so that the near-surface temperature inversion became less intense (approximately 2.5 K in 50 m). This near-surface inversion was capped by a less stable layer with a potential temperature gradient of 8.8 K/km For comparison, this potential temperature gradient is slightly less stable than an isothermal temperature gradient of 10 K/km.

Tethered balloon observations on JD 277 were halted because of strong winds after the 1941 PDT sounding. Doppler sodar wind data were, however, taken continuously during the experimental nights and were useful in supplementing the Tethersonde® data and in characterizing temporal changes in valley wind system structure. As an example of this data, Doppler-measured wind vectors and along- and cross-valley wind component analyses are presented in Figure 10 for the night of JD 277-278. These time height sections were composited from

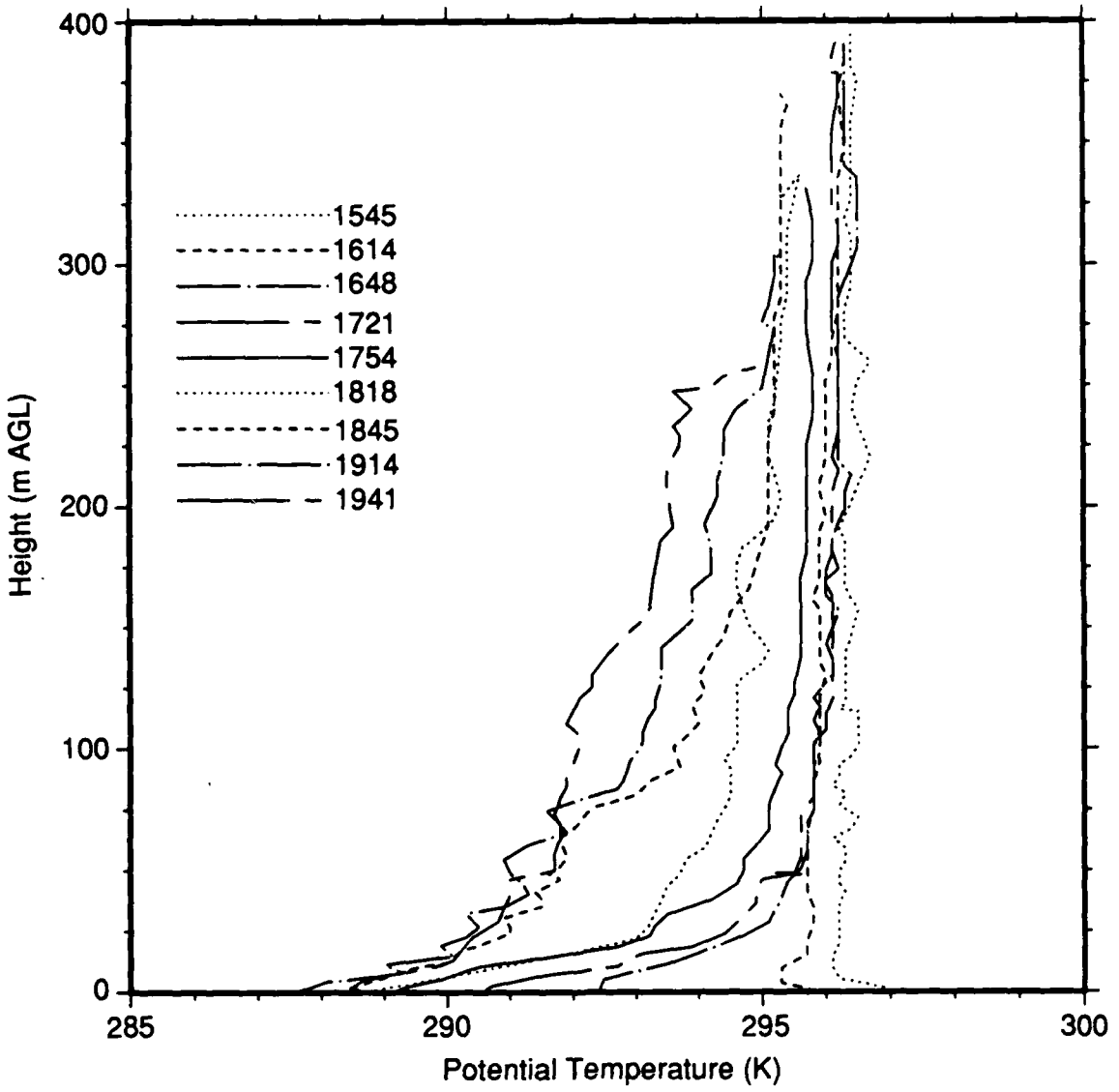

FIGURE 8. Sequence of Tethered Balloon Temperature Profiles, JD 277. Sounding times (PDT) are indicated in the legend.

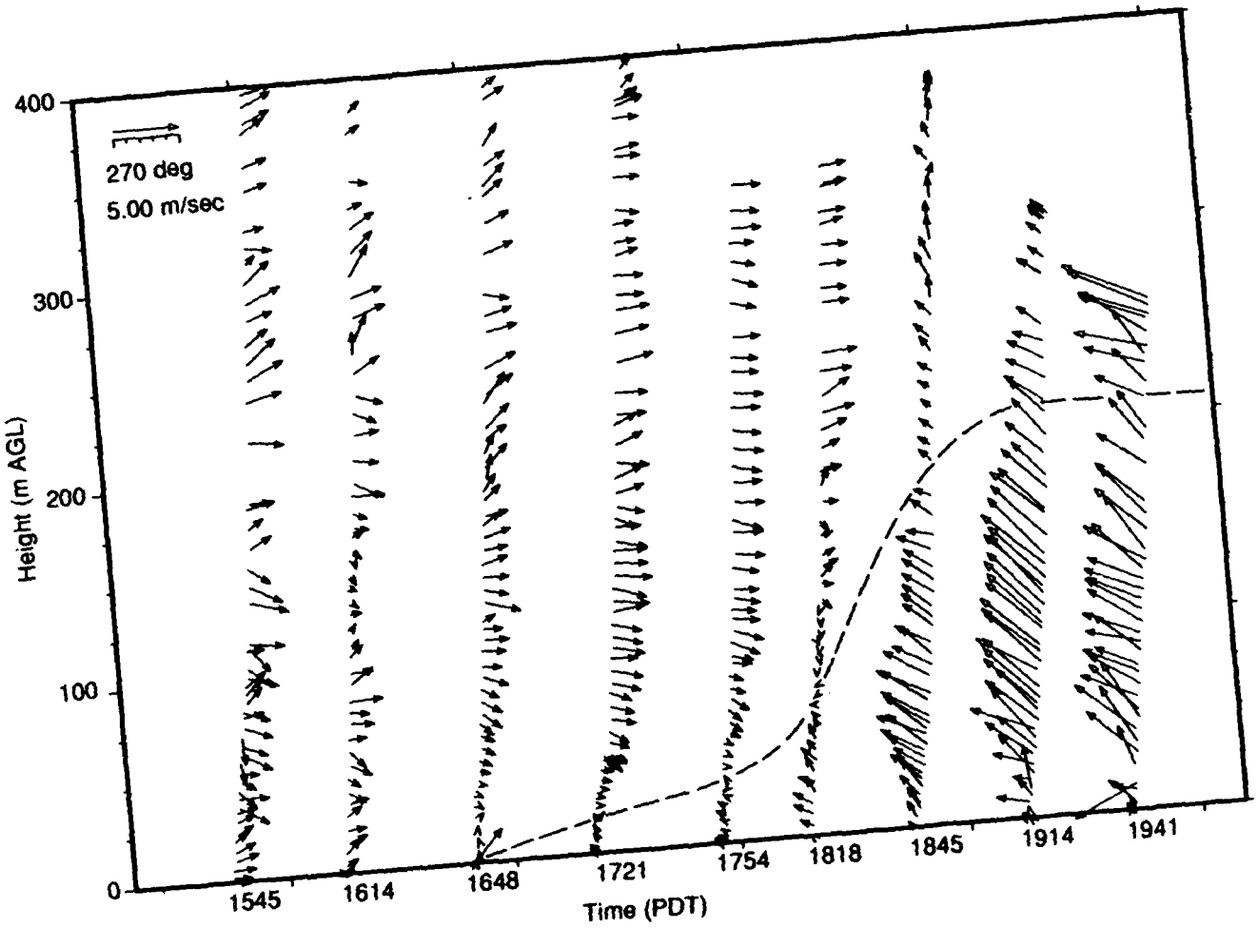

FIGURE 9. Tethered Balloon Wind Profiles, JD 277. The top of the down-valley flow region in the valley is indicated by the dashed line.

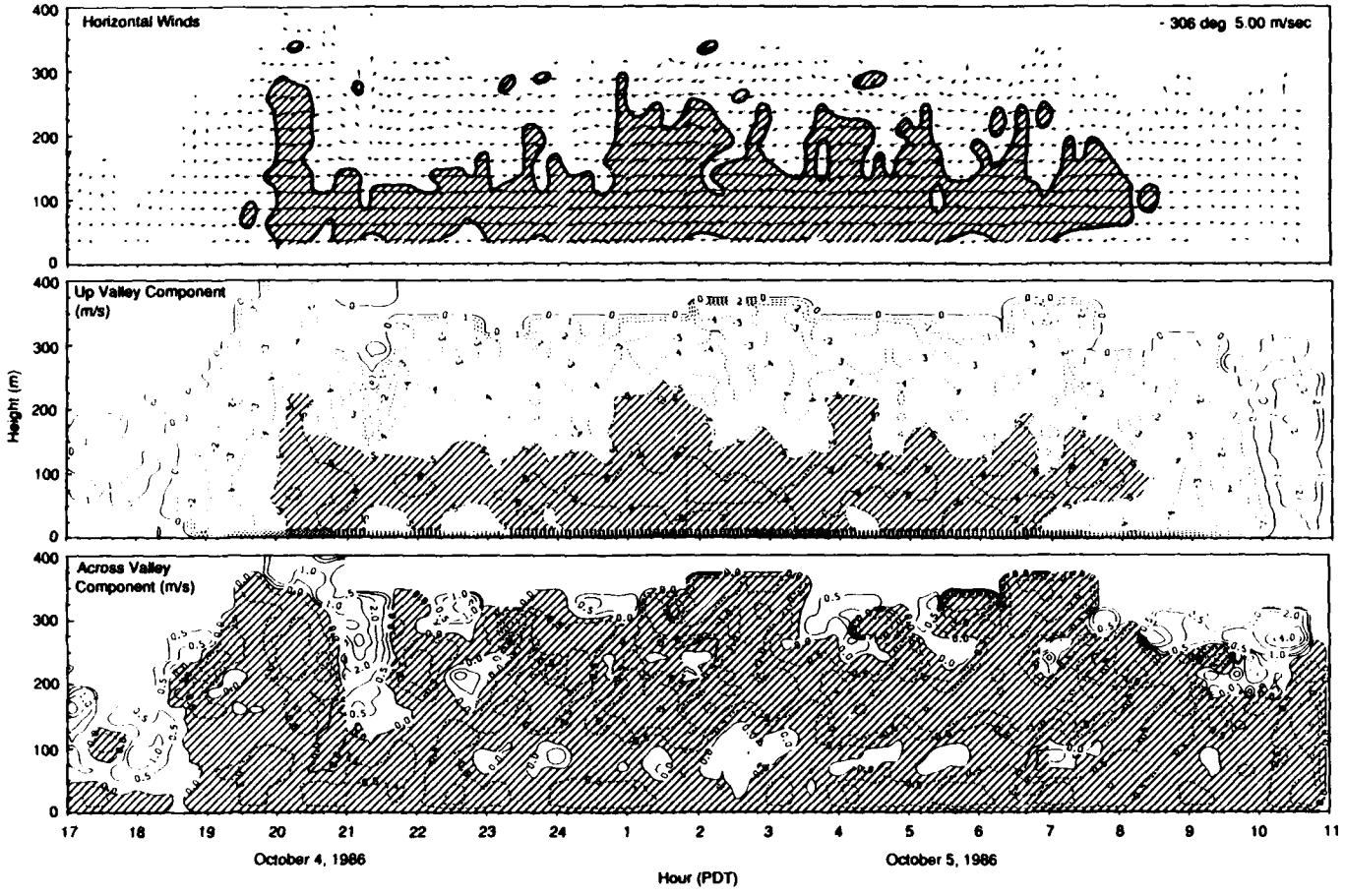

FIGURE 10. Doppler-Derived Winds, S. Fork Touchet Valley, Julian Date 277-278. The upper panel shows vector winds, with wind speeds above 5 m/s shaded. The middle panel shows up-valley wind components (m/s), with down-valley wind speeds over 5 m/s shaded. The bottom panel shows cross-valley wind speeds (m/s). Positive values and shading indicate wind components blowing toward the west sidewall.

analyses of five separate time periods; because of the contouring software used, a slight mismatch in the analyses occurs at the boundaries of the time periods. Also, winds in a shallow layer near the ground are not accurately represented because of the sodar "dead-time" following a sound pulse. Finally, the range of the sodar varies with time according to the turbulence structure in the upper parts of the sounding, so that one should use caution when interpreting wind measurements at upper levels.

The wind analysis in Figure 10 shows a rather typical example of nocturnal valley winds. The down-valley winds are initiated between 1800 and 1900 PDT and reverse to up-valley around 1000 PDT. Nocturnal winds are strongest (6 to 7 m/s) at about the 75-m level. Winds in the lower levels of the valley atmosphere tend to be aligned very well with the valley's longitudinal axis. On the night of JD 277, cross-valley winds were generally less than 0.5 m/s and tended to blow toward the west sidewall. At the level of the jet, there is a tendency for cross-valley winds to be blowing toward the east sidewall.

Evolution of Valley Temperature and Wind Structure on JD 278-279

Figure 11 shows temperature structure evolution on JD 278. Temperature profiles on this night (and other nights as well) evolved initially as described for JD 277, but unusual and distinctive temperature structure layers appeared in the final soundings. These temperature structure layers are quite similar in form and behavior to layers that developed during an evening transition period in Colorado's Eagle Valley, as described by Whiteman (1986). Specifically, a constant potential temperature layer developed above the surface inversion layer. This constant potential temperature layer was capped by a strong potential temperature jump. In the Eagle Valley case, these special structural features were transitory, observed only during the evening transition period, and were hypothesized to be closely related to convergence of downslope flows over the valley center from the opposite sidewalls. The constant potential temperature layer was thought to be the layer into which downslope flows converged,

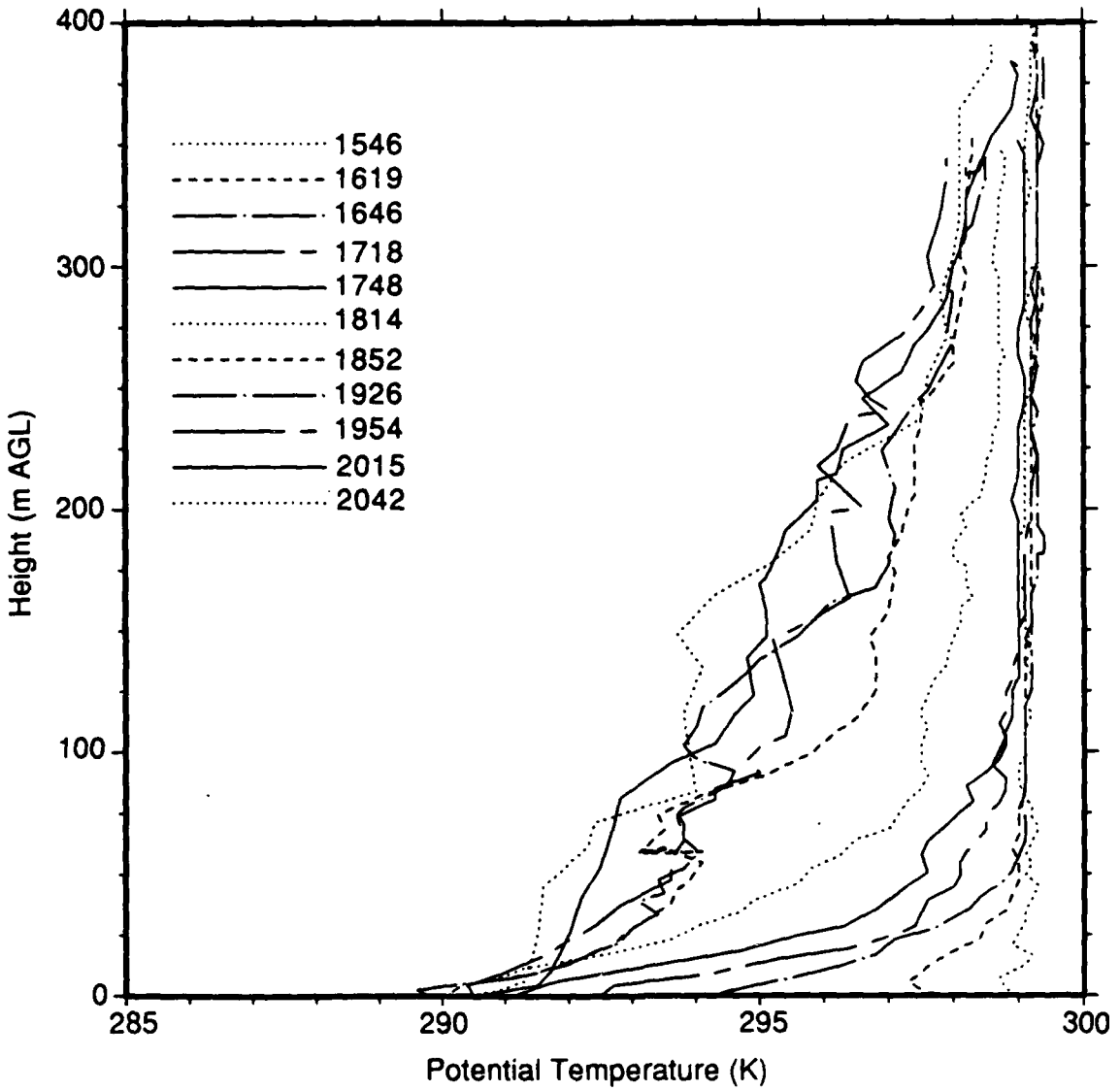

FIGURE 11. Sequence of Tethered Balloon Temperature Profiles, JD 278. Sounding times (PDT) are indicated in the legend.

resulting in a gradual ascent of the top of this layer (i.e., the ascent of the potential temperature jump). In the Eagle Valley, these layers evolved smoothly in time. The Touchet Valley observations show the same structural features and general evolution, but were somewhat more unsteady.

Unfortunately, because strong down-valley winds developed late in the evening, Tethersonde® ascents could not be continued through the night to investigate whether the temperature structure features were transitory. However, on JD 281 a Tethersonde® sounding was made just before sunrise, following a long series of profiles the previous evening. This sounding did not contain the distinctive temperature structure features of the previous evening. The inversion had attained the full valley depth and the inversion had strengthened from 8.5 K (2042 PDT sounding) to 10 K by sunrise. Atmospheric stability had increased from the 2042 PDT sounding at all levels of the profile. An intense ground-based inversion had formed (4.5 K in 45 m), and the atmosphere became progressively less stable with height, attaining an isothermal lapse rate only at the very top of the valley atmosphere. The average potential temperature gradient from 45 m to 225 m was 28.9 K/km. Thus, this sounding suggests that valley inversions gain additional strength, but not depth, between the end of the evening transition time and sunrise, and that special structural features that develop during the evening transition period may be transitory.

However, as will be discussed later in this report, some persistent features of the structure of the slope flows seem to be associated with the presence of these constant potential temperature layers. Indeed, in the particular case of the JD 281 morning sounding, a constant potential temperature layer was absent, but the structure of the slope flow during this period was not representative of the structure for most of the night. This suggests that constant potential temperature layers may, in fact, be present over much of the night. At this time the issue remains unresolved.

Despite the differences in small-scale temperature structure features on the nights of JD 277 and JD 278, the general features of inversion buildup differed little from night to night. This is illustrated in Figure 12, where the growth of inversion depth with time is shown for each of the experimental nights. On JD 276 and JD 280 dual Tethersondes® were flown from different locations in the valley; analyses of both sets of Tethersonde® data are shown in the figure. Inversions were initiated from 1530 to 1745 PDT depending, presumably, on day-to-day differences in valley energy budget, cloudiness and above-valley wind regime. The data show that inversions grew to the full depth of the valley (225 m) in 2 to 3 hours and that further growth was precluded. There is a tendency for the curves in Figure 12 to be concave upward, suggesting that inversion growth is accelerated during the time period when the valley temperature deficit is rapidly mixed upward.

Inversion strength (Figure 13) behaves in a manner consistent with the temperature profile evolution for JD 277. Namely, inversion strength (potential temperature difference between the inversion top and the surface) initially increases rapidly as a shallow layer becomes cooled over the valley floor. This takes place over roughly the first hour of cooling. The inversion strength then increases less rapidly as the shallow temperature deficit is mixed through the valley depth. This reduced rate of cooling continues for 2 or 3 hours until the inversion strength attains about 7 or 8 K.

Cross-Valley Temperature Structure

The initial assumption about the cross-valley temperature structure was that, in the region above the katabatic layer on the sidewall, the temperature would be approximately the same as that in the center of the valley at the corresponding elevation. Another way of expressing this is that the isotherms were expected to be horizontal except near a very thin region next to the sidewalls, where they would turn downward. In that case, a measurement of the temperature at the top of a sidewall tower would provide a good measure of the ambient temperature,

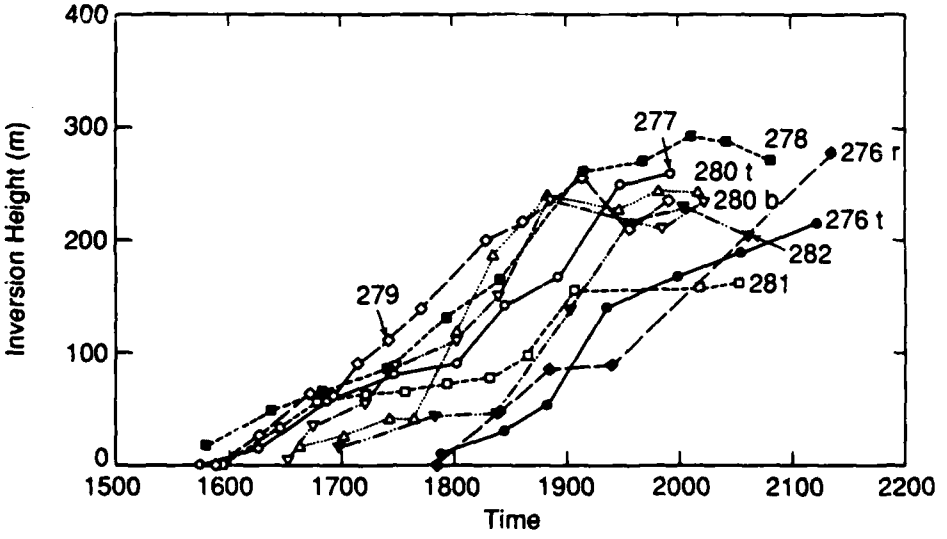

FIGURE 12. Inversion Height Versus Time, S. Fork Touchet Valley, Julian Dates 279 Through 282.

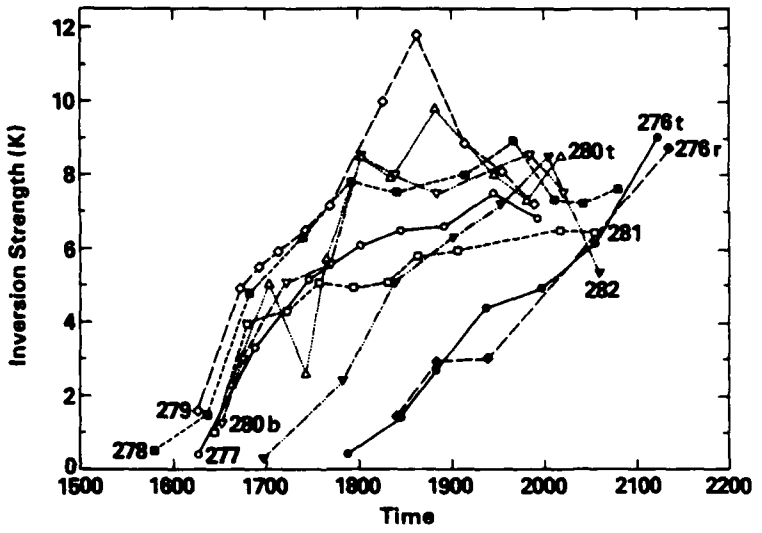

FIGURE 13. Inversion Strength (Temperature at Top of Inversion Minus Temperature at Ground) Versus Time, Julian Dates 279 Through 282.

and the inversion strength measured at the sidewall tower would be nearly equivalent to the temperature difference between the sidewall and the ambient air.

The structure that was actually observed was considerably more complicated. On the east sidewall, at least, the local inversion seemed to be generally well contained by the sidewall towers, so that the temperature gradient near the top of the towers was usually small. However, comparisons of the temperatures at the tops of the towers with those recorded by the Tethersonde® at the same elevation consistently showed differences. At the level of tower A, $T_{teth} - T_{tower}$, averaged 0.71±0.93 K, while at towers B and C the differences were 0.27±0.74 K and -0.09±0.66 K, respectively. The large standard deviations are a bit misleading. When $T_{teth} - T_{tower}$ were plotted individually for each night, there were systematic trends with time that repeated from night to night. Specifically, the temperature differences at towers A and B tended to increase as the evening transition progressed, but at tower C, a clear trend was not obvious. Figure 14 shows an example for the data from tower A. Because of our inability to fly the tethered balloon later in the evening, it is not known whether this behavior persists throughout the night.

A further illustration of the presence of cross-valley temperature gradients is shown in Figure 15. This figure shows time series of temperatures measured at the tops of towers C and E, on opposite sides of the valley, and the main tower in the center of the valley. The tops of all three towers were at approximately the same elevation above the valley floor. The figure covers a 4-hour period for JD 281. The gradients shown are highly variable but significant, and, as will be shown, cause problems in the interpretation and analysis of our data.

It was noted earlier that there were some discrepancies in the temperature values obtained from the Tethersonde® and 61-m tower. However, the horizontal temperature differences between the valley center and the sidewalls were often

on the order of 1 K and would not be eliminated by small adjustments in the temperature values recorded at these locations.

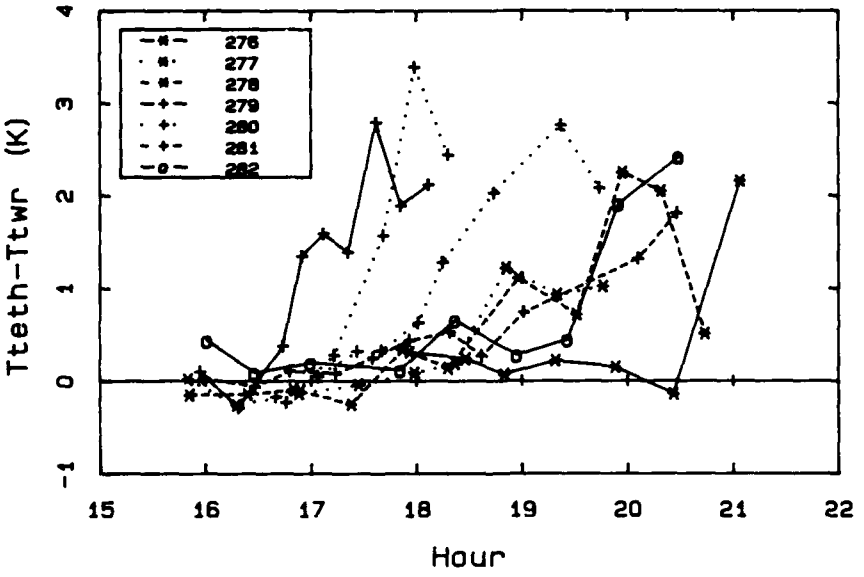

FIGURE 14. Temperature Differences Between Center of Valley (Tteth) and the Top of Tower A. Soundings from two valley locations were made on JD 280.

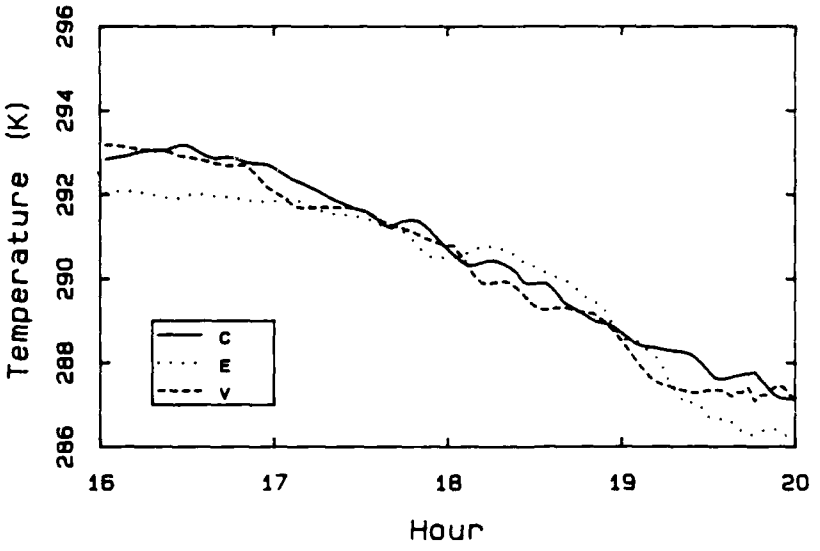

FIGURE 15. Temperatures at Tops of Towers C, E, and 61-m Tower in Center of Valley.

STRUCTURE AND EVOLUTION OF SLOPE FLOWS

CHARACTERISTIC PARAMETERS FOR SLOPE FLOWS

Figure 16 shows wind and temperature profiles at tower B for three 10-min periods on the morning of JD 278. The inversion and the local maximum in the downslope wind speed indicate the presence of katabatic slope flows. These flows persisted for most of the night, as shown in Figure 17, and were found on all nights of our experimental period. However, the relative magnitudes of the downslope winds and the strengths and depths of the inversions varied with time and tower location, and some means of characterizing these variations is needed.

Descriptions of slope flows over simple slopes have made use of a variety of parameters that succinctly summarize some of the principal features of the flow. These include scale heights, scale velocities, buoyancy or temperature deficits, inversion depths, heights of the wind speed maximum, etc. Similarly, in flows down valley sidewalls, it would be useful to characterize the depth, strength, and structure of the local inversion and the downslope wind component in terms of a few parameters.

By assuming a constant eddy diffusivity, Prandtl (1942) derived analytic expressions for the wind and temperature profiles that could be described in terms of three parameters: a velocity scale u_c, a temperature scale θ_0, and a depth l. In this formulation the downslope velocity, u, is given by

$$u(n) = u_c \sin(n/l) \exp(-n/l) \qquad (1)$$

where n is the (normal) distance from the surface, and the deviation from the ambient temperature is given by

$$\theta'(n) = \theta_0' \cos(n/l) \exp(-n/l) \qquad (2)$$

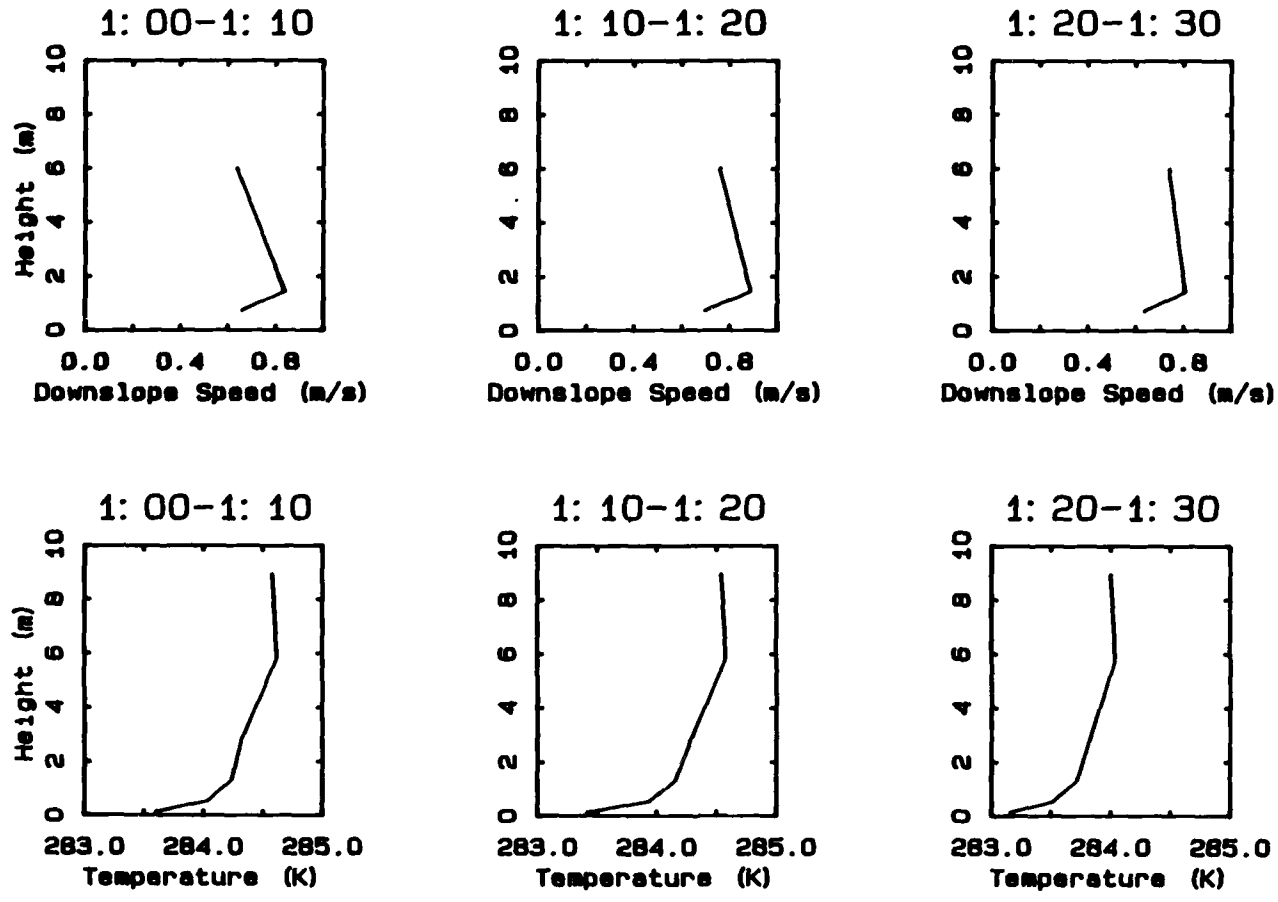

FIGURE 16. Wind and Temperature Profiles at Tower B During Three 10-min Periods on Morning of JD 278.

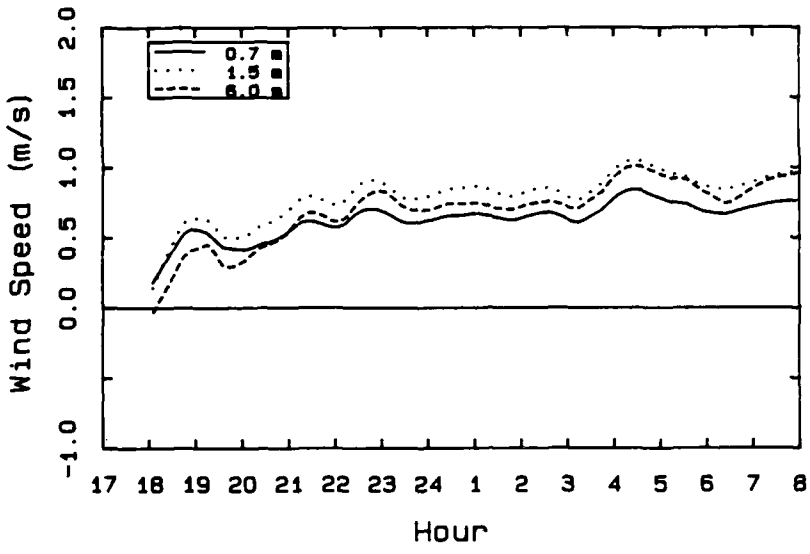

FIGURE 17. Downslope Wind Components at Three Heights on Tower B During Night of JD 277-278.

Filliger et al. (1987) calculated θ_0 and I using a least squares fit to their temperature data, and then used their wind data to calculate u_c; the data were collected near the bottom of a long slope (995 m below the summit) in Switzerland. A similar approach was tried with our data. However, the Prandtl profile gave a poor representation of the shape of our observed temperature profiles near the tops of the sidewall towers. The fit to the velocity profiles was also poor, although the presence of ambient cross-valley winds may have been partly responsible for this. In any event, the Prandtl approach was abandoned in favor of a more promising one.

For the east sidewall, there was considerably better success in fitting the temperature profiles with an expression of the form

$$T(n)=T(9m) + \Delta T \cdot \exp(-n/h) \qquad (3)$$

where ΔT is the inversion strength and h is a measure of the inversion depth. (In discussions to follow, we will refer to ΔT and h as the inversion strength and inversion depth, respectively, although h is more properly an e-folding length rather than an inversion depth.) An example is shown in Figure 18, where $[T(n)-T(9\ m)]/\Delta T$ is plotted on the abscissa and n/h is plotted on the ordinate for data obtained at tower A on the night of JD 278-279. The line is the exponential curve given by Equation (3).

The inversion was generally contained within the 9-m height of the towers on the east sidewall, but not on the west. Figure 19 gives an example from data collected at tower F, also on the night of JD 278-279. The exponential fit is not as good as at tower A, and the temperature is still increasing noticeably with height at the top of the tower. Even so, the exponential parameters are useful in providing an approximate description of the temperature profile. It is also worth noting that even though the Prandtl formulation was not as useful, there are very good correlations between l and h and between θ_0' and ΔT, with generalized correlation coefficients near 1.0 in both cases.

Attempts to find a similarly useful set of parameters to describe the wind profiles were much less successful. There were three principal problems. The first was that three levels of wind measurements on each of the sidewall towers was simply not sufficient to resolve the shapes of the wind profiles. While there was generally clear evidence of a low-level maximum in the downslope wind component during significant portions of the evening and night, its height and magnitude could not be determined. Adding additional levels of wind measurement at each tower was not possible with the data loggers available to us because there were insufficient input channels for recording the output from another anemometer. Second, the highest measurement level (~ 6 m) does not seem to have been high enough to lie above the katabatically driven layer. Finally, while the wind measured at the center of the valley frequently showed a negligible cross-valley component, this was not always the case. Moreover, it is

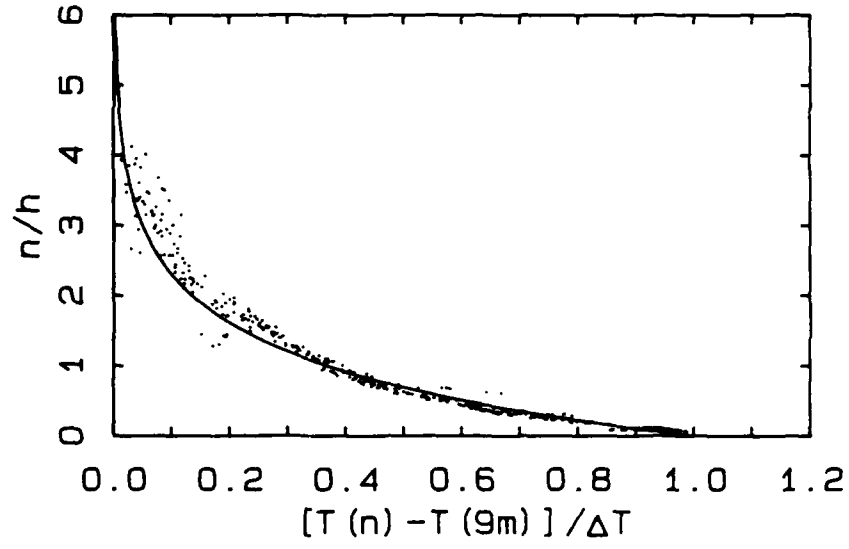

FIGURE 18. Scatter Plot of Temperature Differences on Tower A, Normalized by Inversion Strength ΔT, as a Function of n/h. Line is Equation (3).

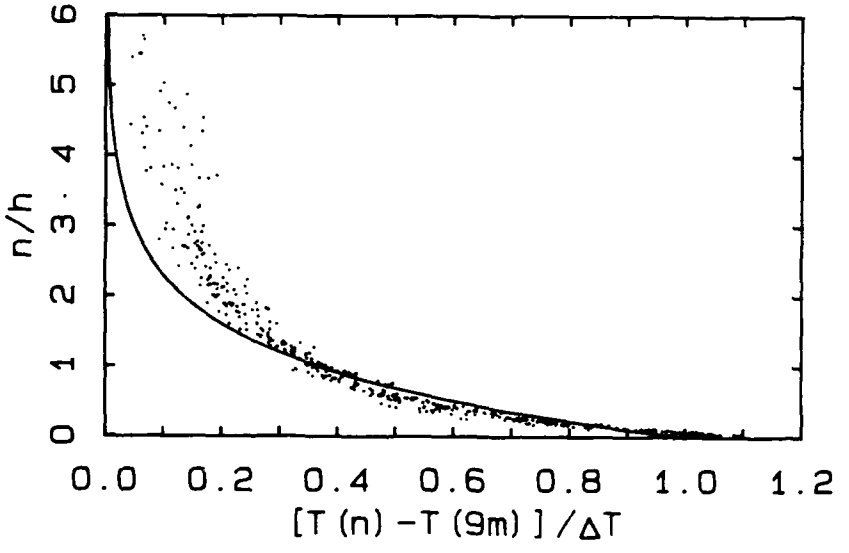

FIGURE 19. Scatter Plot of Temperature Differences on Tower F, Normalized by Inversion Strength ΔT, as a Function of n/h. Line is Equation (3).

not obvious that the ambient winds at the valley center were exactly the same as at the valley sidewalls. This ambiguity in the source (katabatically driven or ambient) of the downslope wind component and the lack of vertical resolution in the measurements made it impossible to assign either a magnitude or depth scale to the sidewall wind data.

Although a suitable magnitude or depth scale for the katabatic wind was not found, two other measures of the katabatic wind can provide some qualitatively useful information. The first, and simplest, is the magnitude of the downslope wind speed at the second level (~1.5 m) at each tower. This may well be affected by the ambient valley winds, and the relative position, e.g., (n = 1.5 m)/h, in the profile at each tower may vary from tower to tower and from one time to another, but it does give some measure of the katabatic wind. It is also possible to make a rough attempt to remove the influence of any unknown cross-valley wind component from the katabatic component by defining an adjusted slope wind

$$U_{adj} = U(2) - [V(2)/V(3)] \cdot U(3) \qquad (4)$$

where U represents a downslope wind component, V a cross-slope (down-valley) wind component, and (2) refers to the second level and (3) to the top level of anemometry on each tower. This approach assumes that the top-level wind is above the katabatic flow, that the contributions of the cross-valley wind and the katabatic wind to the downslope wind component are additive, and that the ratio of the cross-valley winds at the top two measurement levels is equal to that of the along-valley winds. These assumptions may not be very good ones in many cases, and the adjusted wind must be used with caution.

DEPENDENCE OF SLOPE FLOW PARAMETERS ON TIME AND VALLEY METEOROLOGY

Time Relationships

Understanding of the propagation of shadows through the valley during the evening transition period is essential for interpretation of the meteorological data. Sunset times are given in Table 3.

Local sunset times for towers A, B, and C in Table 3 were determined visually by an observer on the valley floor. Sunset times for towers E and F were estimated from the time when net radiation dropped suddenly. A close relationship is expected between the sign reversal of net radiation and the initiation of solar shading on the west sidewall because the sun is high in the sky when shading occurs.

TABLE 3. Local Sunset Times on JD 280 at Base and Top of Sidewall Towers

Tower	Tower Base (PDT)	Tower Top (PDT)
A	1802	1807
B	1740	1745
C	1710	1714
E	1416	----
F	1531	----

Astronomical sunset, i.e., sunset on a hypothetical unobstructed horizontal surface at the latitude and longitude of the field site, is 1822 PDT. As seen in the table, local sunset on the west sidewall is much earlier than astronomical sunset, but local sunset at the uppermost tower on the east sidewall occurs only 20 min in

advance of astronomical sunset. At site E local sunset occurs 3 hours and 46 min before its occurrence at site A. Sign reversal of net radiation, the buildup of a temperature inversion over the slope, and the development of downslope flow occur much earlier on the west sidewall than on the east sidewall. Observations on the valley floor show that the valley temperature inversion begins to build up at about 1600 PDT, nearly 1 3/4 hours after sunset occurs at site F. The buildup of the valley temperature inversion begins before the daytime up-valley flows are reversed. Reversal of the daytime up-valley winds through the entire valley depth occurs at about 1630 PDT. The shadow of the ridge west of the valley moves slowly down the west sidewall, across the valley floor and up the east sidewall. Thus, tower C is the first of the east sidewall towers to be shaded, tower B is second, and tower A is last.

Sidewall Inversion Strength

The nocturnal period at the east sidewall can be conveniently divided into two portions, a transition period in the first hour or so after local sunset and an approximately steady-state period that persists throughout the remainder of the night until sunrise the next morning. During the transition period, the sidewall inversion strengths generally reached their maximum values and then decreased to roughly constant values for the remainder of the night, although there were occasional periods in the early morning hours when the inversion strength might increase temporarily. At tower A the maximum strengths ranged approximately between 2.5 and 5 K, at tower B the range was about 2 to 4.5 K, and at tower C was approximately 1.5 to 2.5 K. For the remainder of the night after the evening transition, the inversion strengths at towers A and B were generally quite similar (~1.2 K) and about 50% greater than at tower C (~0.8 K). Figure 20 gives an example of the time evolution of the sidewall inversion strengths for JD 281-282.

The existence of the cross-valley temperature gradients described previously has made it difficult to identify a useful parameter that characterizes the valley meteorology. Originally it was hoped that some combination of wind speed and a

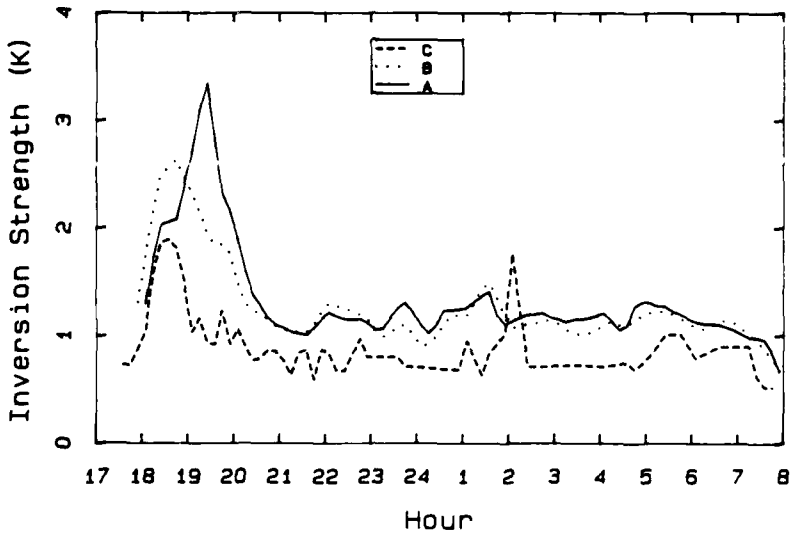

FIGURE 20. Inversion Strengths at Towers A, B, and C on Night of JD 281-282.

temperature difference between the valley center and the sidewall katabatic layer might be used to predict the magnitude of the katabatic wind. However, the existence of a temperature gradient between the valley center and the air above the apparent katabatic layer makes such an approach problematic. Examination of the sidewall data suggested, however, that the valley wind speed alone was a significant factor in determining the slope flow characteristics.

Figure 21 shows a scatter plot of the inversion strength at tower A as a function of the along-valley wind speed at the elevation of tower A, as determined from the sodar measurements, for all six nights of the experimental period. Also shown are means and standard deviations of the inversion strengths for each 1-m/s speed interval. Although there is considerable scatter in the data, particularly at the lower wind speeds, the trend of decreasing inversion strength with increasing wind speed is clear. The lower speeds were usually found during the evening transition periods; after this time, the wind speeds in the valley increased and the

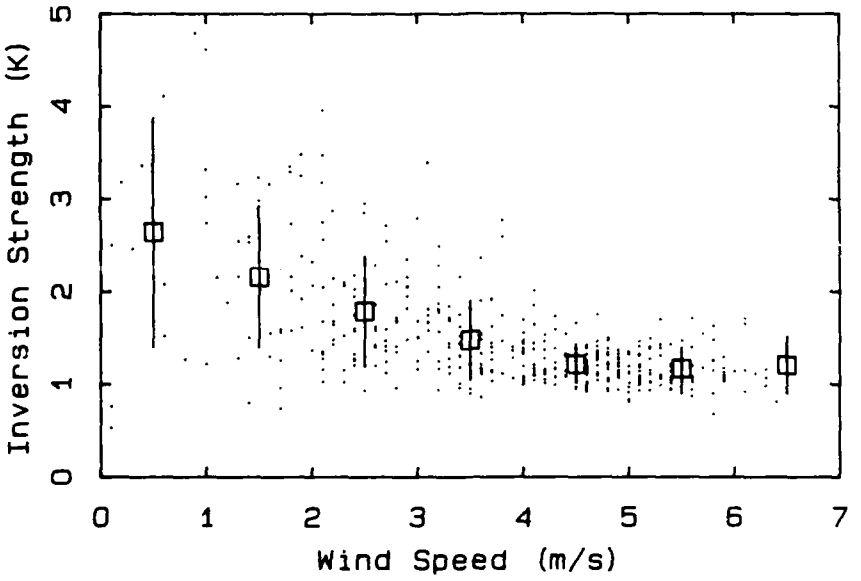

FIGURE 21. Scatter Plot of ΔT at Tower A Versus Down-Valley Wind Speed at Elevation of Tower A. Boxes: means; lines: standard deviations.

inversion strength on the sidewall decreased. There is only one instance of an inversion strength as strong as 2 K when the along-valley wind speed was 4 m/s or higher. It appears that a low valley wind speed is a necessary condition for a strong sidewall inversion to form. A low valley wind speed is not a sufficient condition, however, as can be seen from the wide range of inversion strengths found for speeds less than 4 m/s.

The behavior at tower B is quite similar, but at tower C there are some significant differences (Figure 22). As noted above, the largest inversion strengths are much smaller than at towers A and B, and the steady-state strengths are weaker as well. Figure 22 also shows a relative scarcity of data for low wind speeds. This arises for two reasons. First, sodar echo returns from the lower levels were generally noisier in light winds, and the data recovery was not as good as at higher elevations. More significantly, the down-valley winds developed relatively quickly at the lower elevations, so that by the time an inversion began to form at tower C, the ambient winds at that level were already well established.

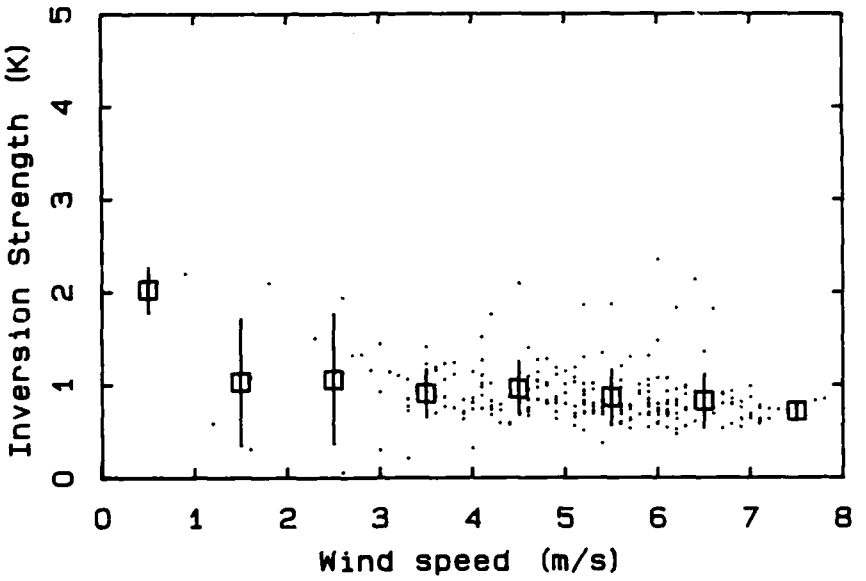

FIGURE 22. Scatter Plot of ΔT at Tower C Versus Down-Valley Wind Speed at Elevation of Tower C. Boxes: means; lines: standard deviations.

Thus, there seem to be two features that contribute to the weaker inversions at tower C. First, the ambient winds at this level tend to be higher than at the levels of towers A and B. Figure 23 shows an example of this for the nights of JD 277-278. This results in greater turbulent mixing, thereby reducing the strength of the inversion. However, even for similar ambient wind speeds the inversion strengths are weaker, as can be seen by comparing Figures 21 and 22. A possible explanation has been given by Manins and Sawford (1979), who developed a layer-integrated model for drainage winds over simple slopes. Their model showed that the inversion strength decreases with increasing slope distance from the crest of the hill, and that this decrease is accentuated as the ambient stability increases. They argued that cooled air moving down the slope encounters denser ambient air and a larger fraction of the cooling is required to maintain the buoyancy deficit in the cooled layer. This appears consistent with the observations made at Dayton; however, on Rattlesnake Mountain, there was no consistent trend with downslope distance in the behavior of the inversion strength (Horst and Doran 1986). The reason for this difference is uncertain, but

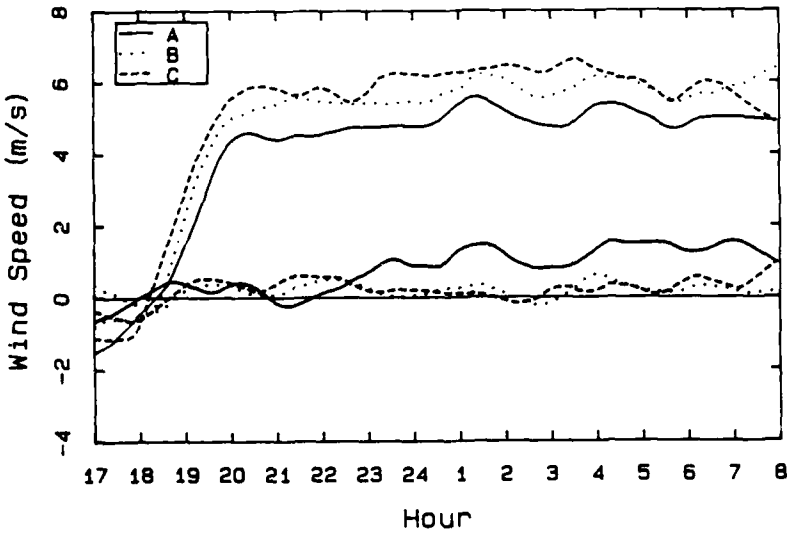

FIGURE 23. Wind Speeds at Elevations of Towers A, B, and C on Night of JD 278-279. Upper curves: along-valley winds; lower curves: cross-valley winds.

may be related to the much stronger stratifications found in the Dayton valley compared to those at Rattlesnake Mountain. Any tendency for ΔT to decrease with increased stability would thus be accentuated at the Dayton site.

Sidewall Inversion Depth

During the evening transition period the inversion depths (i.e., the e-folding depth defined earlier) at all three towers increased so that their maximum values were obtained around 2030 PDT. Typical maximum depths were around 3 m at tower A and 2 m at towers B and C. After this initial period the depths decreased slowly to around 2 m for tower A and 1 m for towers B and C. The behavior at towers B and C was generally similar except that tower C often showed an increase in h to around 1.7 m for a few hours before sunrise. Figure 24 shows an example of the time evolution of inversion depths for the night of JD 277-278.

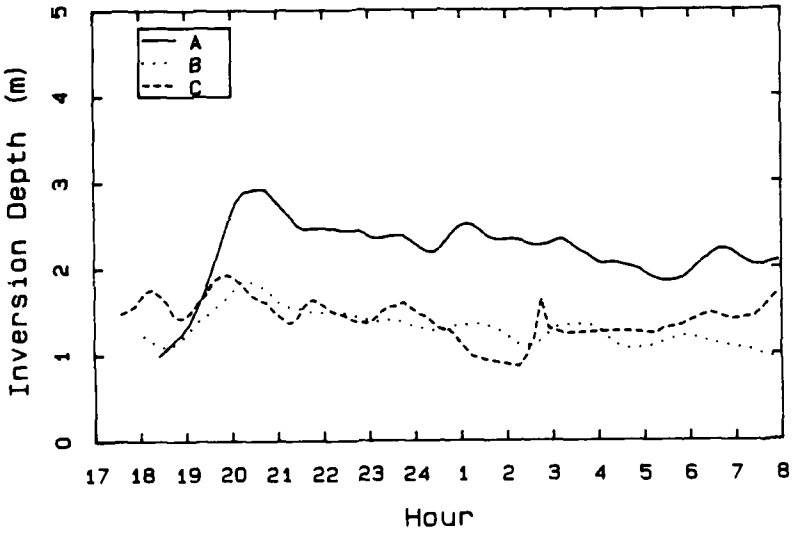

FIGURE 24. Inversion Depths at Towers A, B, and C on Night of JD 277-278.

The dependence of the inversion depth on downslope distance is in marked contrast with that found over simple slopes. It also differs from predictions of models such as the one developed by Manins and Sawford (1979). That model shows the slope flow depth increasing with downslope distance, a result usually found in the Rattlesnake Mountain measurements as well.

Model predictions are not consistent on this point. Manins and Sawford (1979) and Nappo and Rao (1987) both calculate the behavior of h', the momentum depth for katabatic flows. The Nappo and Rao model is a finite difference model and not a layer-integrated one, but they calculate h' from their solutions as well. This depth scale is related to the height to which the katabatic winds extend, and is defined by the set of equations

$$Uh' = \int_0^{\infty} u\,dn' \qquad (5)$$

and

$$U^2 h' = \int_0^{\bar{}} u^2 dn' \qquad (6)$$

Horst and Doran (1986) showed that the momentum depth and the inversion depth are proportional for the conditions that prevail over a simple slope, i.e., relatively weak stratification without significant changes with height. Manins and Sawford's model predicted that the momentum and inversion depths should increase faster with downslope distance as the stable stratification of the ambient atmosphere increases. Nappo and Rao used a constant ground temperature deficit as a lower boundary condition for their thermodynamic equation instead of the constant buoyancy flux condition used by Manins and Sawford. Nappo and Rao also claim that Manins and Sawford's assumption of an entrainment rate independent of stratification is not justified, and reach a different conclusion about the growth of h'. From their calculations, they conclude that h' still increases roughly linearly with slope distance if the stratification is increased, but also assert that the magnitude of h' will be smaller for a given value of slope distance.

Neither model deals with the case of ambient stratification changing with elevation, as occurs in the valley, and in such circumstances it is not obvious that the momentum and inversion depths will behave similarly. However, in the presence of downslope ambient winds the momentum depth is difficult to define or measure. Even if there had been no ambient winds, our wind measurements apparently did not extend far enough above the slope to lie above the katabatic flows, so a determination of the momentum depth would not have been possible. This issue is discussed further in the section describing the results of numerical simulations carried out for this project.

The area under the temperature inversion profile is proportional to the total buoyancy deficit driving the katabatic slope flow. In the case of the exponential temperature profile, this area is equal to the product of the inversion strength ΔT

and the inversion depth scale h. The product $h \cdot \Delta T$ decreases with downslope distance, from a typical value of 2.5 m-K at tower A to 1.5 m-K at tower B and 1 m-K at tower C. In contrast, on Rattlesnake Mountain the total buoyancy deficit increased monotonically with downslope distance, in keeping with the predictions of the model of Manins and Sawford.

The observed behavior of the temperature structure is summarized in Table 4. The first column lists the predictions of the Manins and Sawford model for the behavior of three quantities, the inversion depth (actually, the momentum depth, which is proportional to the inversion depth in their model), the inversion strength, and the buoyancy deficit. The second column lists the observed behavior on Rattlesnake Mountain at three towers, A, B, and C, placed in the same relative order (top to bottom) as at Dayton. The column is labeled as "Simple Slope." The third column refers to the observations on the valley sidewall at Dayton. The notation A > B for inversion depth, for example, means that the inversion depth at tower A is greater than that at tower B.

TABLE 4. Relative Values of Inversion Depths, Inversion Strengths, and Buoyancy Deficits from Predictions for a Simple Slope, Measured on a Simple Slope, and Measured on a Valley Sidewall

	Model prediction	Simple Slope	Valley Sidewall
Inversion Depth	A < B < C	A < B < C	A > B ~ C
Inversion Strength	A > B > C	A ~ B ~C	A ~ B > C
Buoyancy Deficit	A < B < C	A < B < C	A > B > C

Comparisons of the relative values of these parameters found on the west sidewall of the valley are not as straightforward. The three towers were not

arranged along a line as was true for the east sidewall towers, nor was the slope as uniform as the east slope, particularly in the area of towers D and E. The inversion strength at D was generally larger than that found at the other towers by as much as 1 K or more, while at towers E and F values were closer to those obtained on the east sidewall. The inversion depths at all three towers on the west sidewall tended to be somewhat larger than on the east sidewall, particularly at tower D where values of 4 m or more were found. During the transition period the inversion strengths on the west sidewall were also larger, with values of over 6 K found in some instances. As noted previously, sunset occurred significantly earlier on the west sidewall than on the east sidewall, so that the inversions also formed earlier on the west wall. Unequal heating of the two sidewalls, arising because of their differing surface vegetation and exposure to solar radiation, no doubt contributes to the differences in inversion and katabatic wind characteristics over the two sidewalls. It is likely that this differential heating is also responsible for the development of the cross-valley temperature gradients described previously.

Downslope Winds

Wind measurements were made at nominal heights of 0.7 and 1.5 m at all three towers on the eastern sidewall, with a third measurement at 3.5 m on tower A and ~6 m at towers B and C. The wind at the 1.5-m level often had the largest downslope component, so that even though there is not sufficient resolution in our wind measurements to identify the height of a downslope jet, it is reasonable to look at the 1.5-m level winds as a rough indicator of the strength of the katabatic flow. In the discussion to follow, unless specified otherwise, references to a downslope component are to be understood as the downslope component at ~1.5-m height at each tower.

At tower B, the downslope component had typical values in the range of 0.6 to 0.8 m/s for most of the nights. At tower A the downslope component was generally a few tenths of a meter per second lower, but at tower C the downslope

component was much more variable than at A and B. Figure 25 shows the time dependence of the downslope wind component on the night of JD 277-278; similar fluctuations were observed on the other nights of the experimental period.

Because the quantity $h \cdot \Delta T$ is proportional to the total buoyancy deficit driving the katabatic flow, a correlation between that quantity and the strength of the katabatic flow was expected. This expectation was realized, but only when the down-valley winds were relatively weak. An example is given in Figure 26, which shows a scatter plot of downslope winds as a function of $h \cdot \Delta T$ at tower B, for cases in which the along-valley winds in the center of the valley were less than 2 m/s. For down-valley winds stronger than 2 m/s (Figure 27) the trend exhibited in Figure 26 vanished. This shows that once the valley wind systems are well established, fluctuations in the sidewall inversion structure have little effect on the downslope wind component. It is possible that the height of the

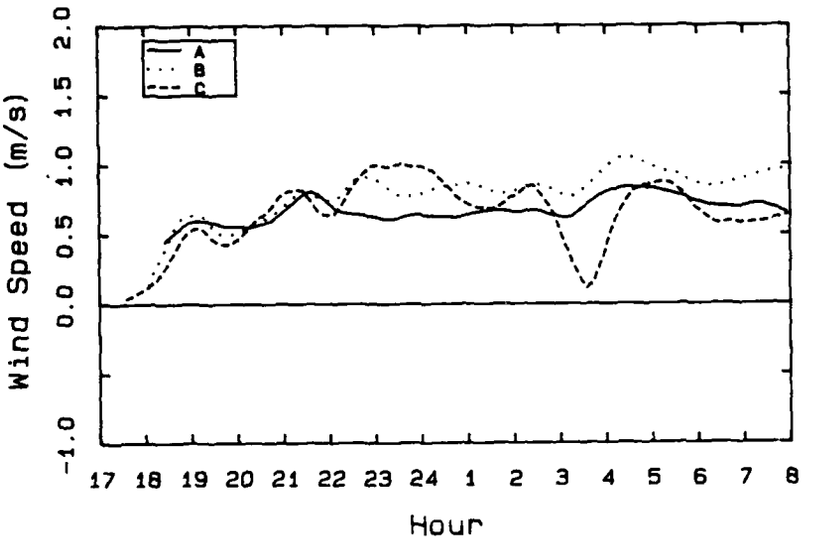

FIGURE 25. Downslope Wind Speeds at 1.5-m Height at Towers A, B, and C on Night of JD 277-278.

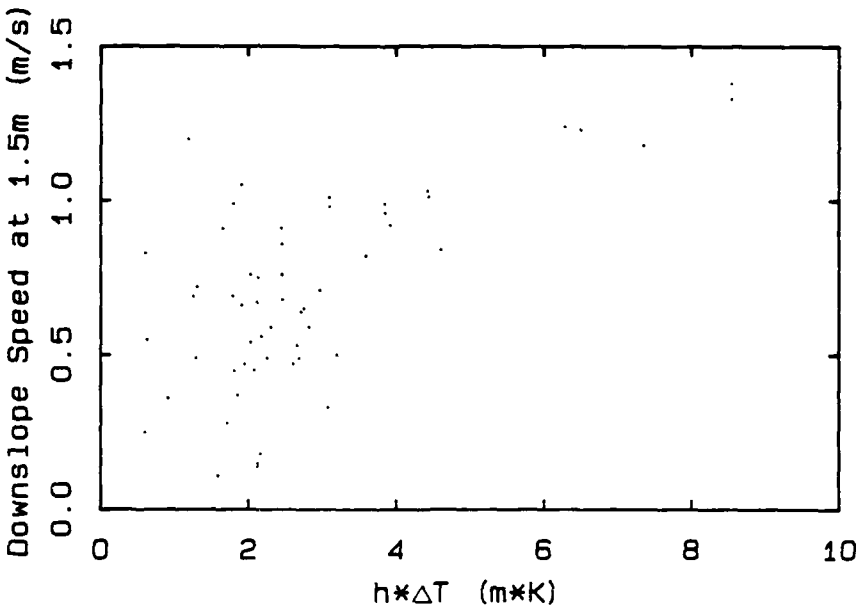

FIGURE 26. Scatter Plot of Downslope Wind Speeds at 1.5-m Height at Tower B as a Function of h·ΔT for Along-Valley Winds Less Than 2 m/s.

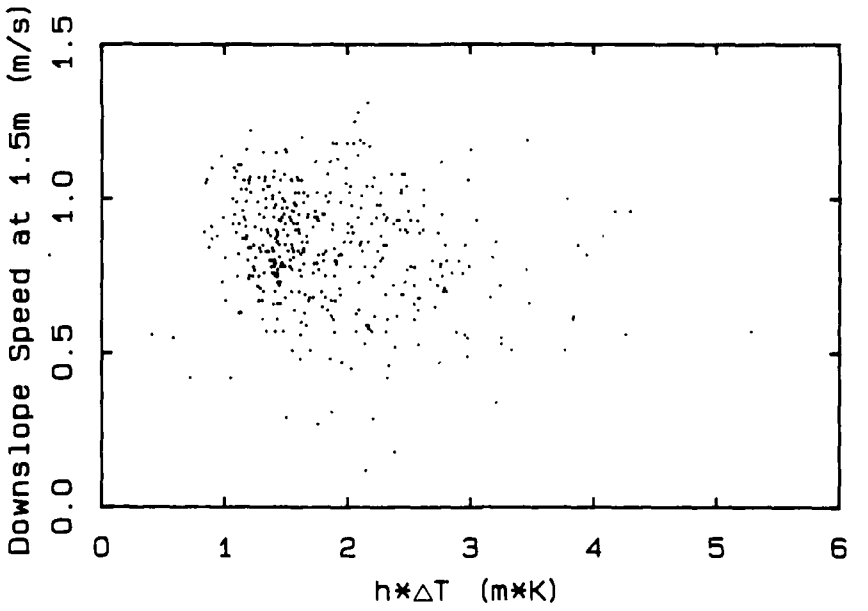

FIGURE 27. Scatter Plot of Downslope Wind Speeds at 1.5-m Height at Tower B as a Function of h·ΔT for Along-Valley Winds Greater Than 2 m/s.

downslope wind maximum, its peak value, or the total downslope volume flux may depend on the total buoyancy deficit, but these possibilities could not be tested with only three anemometers at each of the sidewall towers.

The adjusted slope wind was defined earlier. It was found to be between two and three times larger at tower B than at tower A. Figure 28 shows an example for the night of JD 278-279. It was noted earlier that the assumptions necessary to make this a useful parameter are tenuous. Moreover, comparisons between tower A and towers B and C are of limited value for this quantity because the top anemometer was at a lower height on tower A than it was for towers B and C. We have included this discussion here for completeness but are not convinced that the adjusted wind speed is a particularly useful parameter for this analysis. However, we note that if the instrument towers had been taller or if one can be otherwise assured that the katabatic layer is contained within the tower's height,

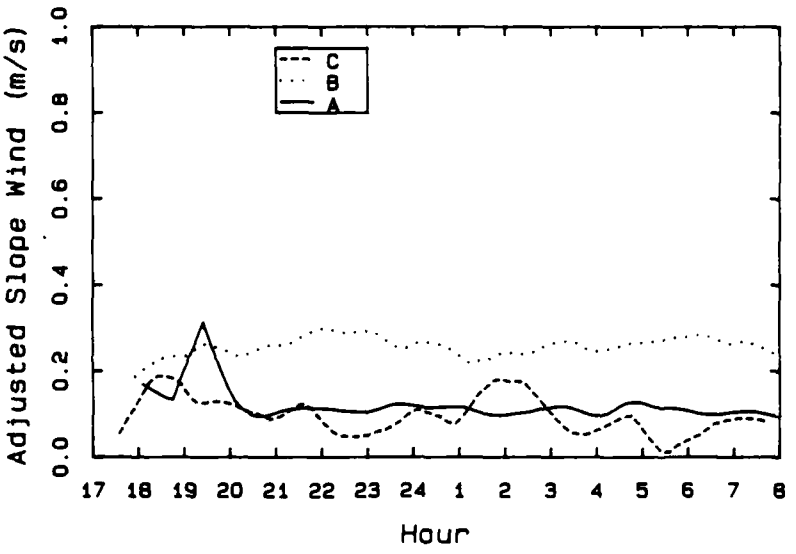

FIGURE 28. Adjusted Slope Winds at Towers A, B, and C on Night of JD 281-282

then this parameter may provide a useful way of reducing the effects of the ambient valley winds in the analysis of the downslope flows. Although the inversion was usually contained by the vertical extent of the thermistors on the towers on the east sidewall, the katabatic flow depths apparently extended beyond the highest anemometers. A complete measurement of the katabatic wind profile would require additional instruments at higher levels to determine their vertical extent and additional instruments at low levels to resolve the local katabatic wind maximum.

The downslope winds at ~1.5 m on the west sidewall were weaker than those observed on the east sidewall, particularly at tower F. Figure 29 shows an example for the night of JD 278-279. The downslope winds appear to weaken around the time that the strong down-valley winds develop, but the winds at tower E show some recovery a short time later. This behavior was observed on several nights, but only for this one tower. The effect is not understood at this time.

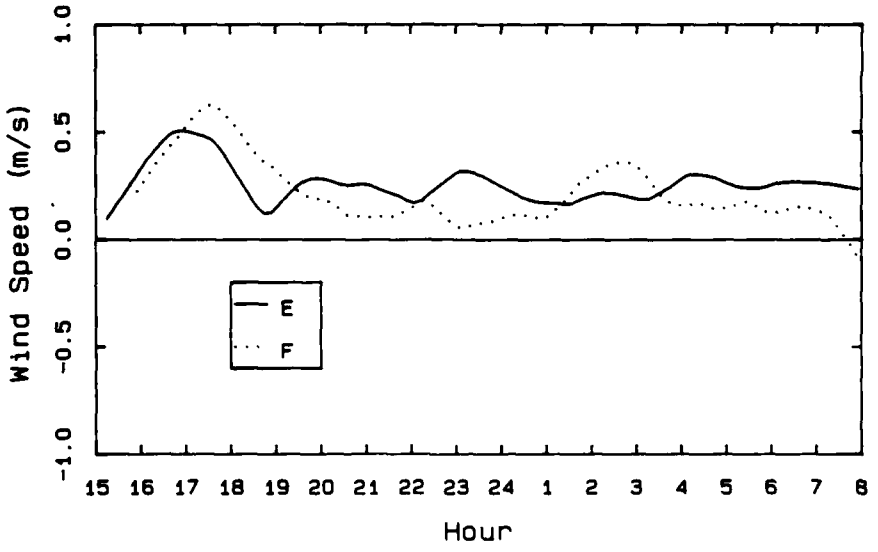

FIGURE 29. Downslope Wind Speeds at ~1.4-m Height on Towers E and F on Night of JD 278-279.

NUMERICAL MODEL

During the course of this research, related complex terrain studies were being carried out for the U. S. Department of Energy's ASCOT program. In that program, a two-dimensional slope flow model was being developed for use in a nested mode with a three-dimensional numerical code; together, the two models would be used to study the interactions of slope and valley flows in some detail. The approach was that the three-dimensional code would provide the ambient, larger scale environment in which the two-dimensional code would operate; the two-dimensional code would, in turn, provide improved resolution near the surface and a lower boundary condition for the larger scale model. It was realized that the two-dimensional code might also be useful in our studies of the slope flows at Dayton. In this case, our observations would be used to describe the ambient environment in which the two-dimensional code would operate.

The model assumes that the slope angle is constant, and the equations to be solved are written in a coordinate system that is parallel (s component) and normal (n component) to the sloping surface. Equations are solved for the downslope wind component u, the cross-slope component v, the turbulent kinetic energy e, and the potential temperature difference θ'. Here, θ' is the difference between the potential temperature in a layer affected by the cooling of the sidewall surface and the ambient potential temperature found in the middle of the valley.

The turbulent exchange coefficients K are derived from the turbulent kinetic energy (TKE) through the equation

$$K_a = C_a l (ae)^{\frac{1}{2}} \tag{7}$$

where l is a mixing length, and the coefficient a has the value 0.733. The constant C_a has values of 1.0, 1.15, and 0.5 for momentum, heat, and TKE,

respectively. This is a simplification of a slightly more complex scheme that depends on the flux Richardson number, as developed by Mellor and Yamada (1982). The model results were found to be rather insensitive to the particular values of C_a used.

A more complete description of the model equations is given in Appendix B.

BOUNDARY CONDITIONS

The boundary condition for the thermodynamic equation describing the behavior of θ' was obtained by specifying the temperature of the air immediately above the ground. These near-surface temperatures were estimated from extrapolations of tower temperature profiles to the surface, and do not, strictly speaking, correspond to the radiating temperature of the soil. However, for simplicity, the term "surface temperatures" will be used for this quantity.

During the course of our observations, both the ambient valley temperature structure and the local sidewall temperature structure changed. Thus, calculations of the katabatic driving term, which depends on θ', should be taken with respect to a varying ambient temperature field. The following approach was adopted. An initial and a final valley temperature profile were chosen, and initial and final sidewall surface temperatures were also selected. During a simulation, the valley and surface temperatures were linearly interpolated in time between their initial and final values. Values of θ' were computed as the difference between the calculated temperatures in the model and the ambient temperatures at that time. The use of linear cooling rates seems to be a useful approximation because the model results depended primarily on the final state of the ambient temperature and wind fields; the initial temperature profile and the rate of cooling had little effect on the results. It was also assumed that there was no initial motion normal to the slope so advection normal to the surface was produced only by katabatically induced winds. This is consistent with our treatment of the valley

temperature structure as an externally imposed boundary condition.

At the upstream boundary (the ridge line), only the ambient temperature was allowed to change; values of u, v, etc. were assumed fixed at their initial values. The downstream boundary (near the valley floor) used a zero-gradient condition in the downslope direction for all quantities. At the top of the model, u and v were set equal to ambient values assumed or measured in the center of the valley. In general it was assumed that there were no cross-valley ambient winds. Sodar measurements showed this was not always true but it was often a good approximation and greatly simplified the construction of the model. In a typical simulation, an initial temperature and down-valley wind field were specified. The model was run for a spin-up period, normally 2 hours, during which the temperature profile was held fixed but other variables were allowed to come to equilibrium. At the end of this spin-up period, cooling of the surface began and the ambient temperature began to change as well. The model time step was 0.5 second.

MODEL TESTING

Two sets of tests were carried out with the model. One set used several ambient temperature profiles of the type that might be encountered over a simple slope, i.e, profiles with constant stratification. The temperature profiles that resulted from these simulations were then fit to the exponential curve described earlier, and values of h and ΔT were computed from a least squares fit to the temperature profiles over the first nine meters above the slope, as had been done with the actual data. The dependence of these quantities on downslope distance was then compared with predictions for the momentum depth from the model of Nappo and Rao (1987). Following the procedure of Nappo and Rao, a constant temperature difference between the sidewall surface and the ambient atmosphere at the same elevation above the valley floor was specified. Manins and Sawford (1979) imposed a constant buoyancy flux as their lower boundary condition, but this condition was not tried for these tests.

For an adiabatic ambient lapse rate, h was found to increase monotonically with downslope distance, while ΔT was found to decrease slightly. When the stability was increased, h increased at a slower rate while ΔT remained essentially constant in the region between towers A and C. The results for h are qualitatively similar to those reported by Nappo and Rao for h', the momentum depth; the momentum depth was also calculated with our model and also showed a monotonic increase with downslope distance. Nappo and Rao did not specifically evaluate a quantity equivalent to ΔT, so comparisons cannot be made with that quantity.

Additional tests were run in which the ambient stratification was allowed to change abruptly with height, as was seen in many of the temperature soundings discussed earlier. It was found that in descending along the sidewall from a region of strong stratification into an adiabatic layer, the scale height h would decrease and then begin to increase again because of the distortion of the temperature profiles in the transition region. This behavior illustrates the sensitivity of the scaling parameters to the details of the ambient temperature profiles in which the katabatic flows develop. In contrast, the momentum depth h' increased more rapidly when the adiabatic layer was entered, as would be expected. Thus, when the stratification changes with height, the two depth scales, h and h', no longer evolve similarly with downslope distance. This is a marked difference from the behavior over simple slopes, where significant changes in stratification are less likely to be found than in valleys.

To test the model's ability to simulate the observed slope flow characteristics, the evenings of JD 277, JD 278, and JD 281 were chosen as test periods. Our final Tethersonde® soundings on those nights were launched at 1941 PDT, 2043 PDT, and 2024 PDT, respectively, and the data obtained on those flights were used to construct final ambient temperature and wind profiles for the model. An adiabatic initial state was assumed. Final surface temperatures at towers A, B,

and C were estimated from extrapolations of the observed temperature profiles on the towers. Surface temperatures in the model were then obtained from interpolations between these locations and estimated extrapolations beyond these points.

The assignment of the final ambient temperature profiles was somewhat difficult. The Tethersonde® soundings showed significant spatial and temporal irregularities. An example is given in Figure 30, which shows portions of three successive profiles on the night of JD 278. The presence of any cross-valley temperature gradients further complicates the problem of choosing the proper ambient state for the model, as will be shown in the examples below.

In practice, piecewise linear approximations for the ambient temperature and down-valley velocity profiles were used. Figure 31 shows the final temperature

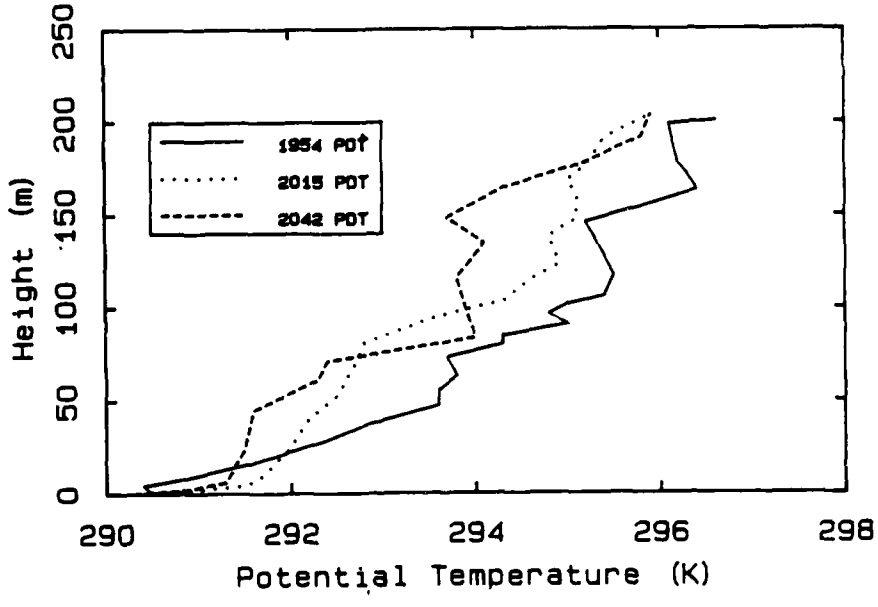

FIGURE 30. Potential Temperature Profiles for Last Three Soundings on Night of JD 281.

profiles chosen for the three simulations. In each case an initial adiabatic profile was assumed. Model results are summarized in Table 5.

The inversion depths at tower A are about 25 to 30% too low for all three simulations. The depths at the other two towers agree reasonably well with observations, and the relative ordering from towers B to C is also reproduced well. For JD 277, the simulated inversion strengths at all three towers agree with observations. The simulations for the inversion strengths on days 278 and 281 are not as satisfactory; for both days, the simulated inversion strengths are too large in most instances. The observed buoyancy deficit, which is proportional to $h \cdot \Delta T$, decreases with increasing downslope distance for all three cases shown in Table 5. The model also showed $h \cdot \Delta T$ decreasing, except for tower A on JD 277 when the low value of inversion depth made the simulated buoyancy deficit at tower A slightly less than at tower B.

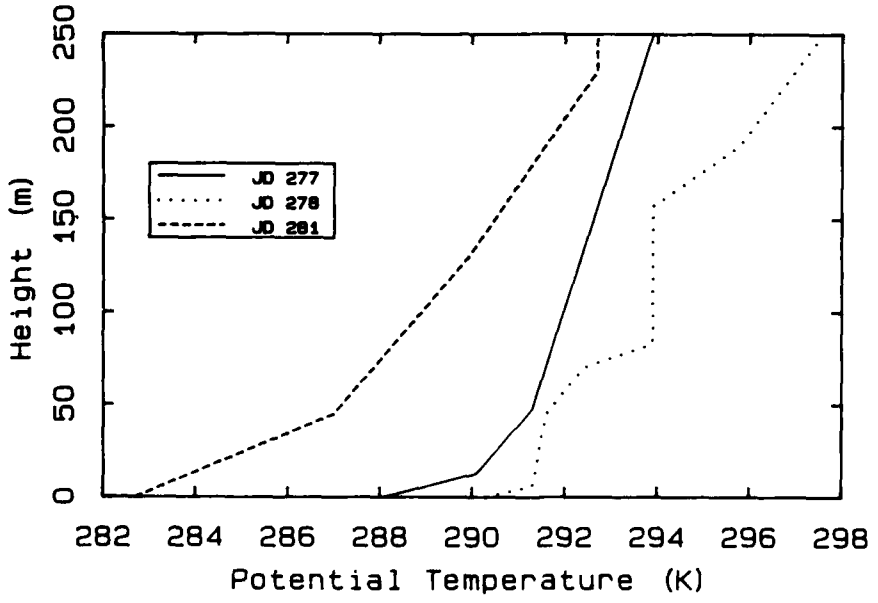

FIGURE 31. Potential Temperature Profiles Used for Simulations of Slope Flows on Nights of JD 277, 278, and 281.

Table 5. Comparisons of Observed and Calculated Values of Inversion Depth h, Inversion Strength ΔT, and Their Product for JD 277, JD 278, and JD 281

	TOWER	OBSERVED			SIMULATED		
		h(m)	ΔT(K)	h*ΔT(m-K)	h(m)	ΔT(K)	h*ΔT(m-K)
JD 277	A	2.3	-1.3	-3.0	1.6	-1.3	-2.1
	B	1.5	-1.4	-2.1	1.6	-1.4	-2.2
	C	2.1	-0.9	-1.9	2.0	-0.9	-1.8
JD 278	A	2.7	-1.4	-3.8	1.9	-2.1	-4.0
	B	2.2	-1.0	-2.2	1.7	-2.1	-3.6
	C	2.1	-0.9	-1.0	1.7	-2.1	-2.0
JD 281	A	1.6	-2.1	-3.2	1.2	-2.7	-3.2
	B	1.2	-1.5	-1.8	1.5	-2.0	-3.0
	C	1.8	-0.9	-1.6	1.7	-0.6	-1.0

The poorer performance of the model in simulating the inversion strengths on JD 278 and JD 281 can be understood in terms of the difficulty of establishing the proper ambient temperature profiles to use on these days. As noted earlier, Tethersonde® measurements often showed significant spatial variations during a flight and from one flight to the next; these fluctuations were particularly severe on the evening of JD 278. We also commented earlier on the temperature gradients between the center of the valley and the sidewall. Figure 14 showed an example of such differences, which can be seen to be larger for the nights of JD 278 and JD 281 than for the night of JD 277. These differences are consistent with the calculated inversion strengths being too high for JD 278 and JD 281. Furthermore, they demonstrate clearly why measurements of the conditions in the center of the valley may not be sufficient to determine the nature of the slope flows.

Accurate estimates for the surface air temperatures are also unavailable except at the three towers. Extrapolations to grid points outside the positions of towers A and C, which are located approximately at grid positions 5 and 10.5, respectively, are essentially educated guesses. This problem is compounded at the downslope end of the model because there is an increase in the actual slope angle below tower C while the model assumes a constant slope angle.

SIMULATED SLOPE FLOWS

Despite some uncertainties, the model captures many of the essential features of the slope flows on the valley sidewalls. As a result, it can be used to examine some of the mechanisms responsible for the observed features. The model can also be used to give additional information on the structure of slope flows that was not measured.

A large number of simulations were performed, using different combinations of ambient stabilities, surface temperatures, and down-valley winds. The inversion depths and strengths defined previously were used to characterize the resultant structure of the slope flows, and a search was made for cases that corresponded to the most commonly observed behavior of these features, *viz.*, ΔT at towers A and B were comparable and bigger than at tower C, while the inversion depth h at tower A was larger than at towers B and C, where the depths were similar.

For the first simulation a set of surface temperature values was chosen, and for all the simulations a fixed potential temperature increment between the bottom of the valley and a point slightly above the ridge line was assumed. The down-valley wind profile was defined as a broad jet with a peak value of 5.4 m/s at a height of approximately 90 m above the valley floor. A series of final ambient temperature profiles was then tested to see which ones yielded acceptable behavior of h and ΔT. As indicated by the first set of tests described above, the form of these profiles proved to be critical. A constant stability between the surface and the

ridge line (Profile 1 in Figure 32) gave a monotonic increase in h from tower A to C (Test 1 in Table 6). However, if regions in which the potential temperature was constant with height were included (Profile 2 in Figure 32), as found in many of the Tethersonde® soundings in the later parts of the evenings, the simulations corresponded much more closely to observations (Test 2 in Table 6).

The surface temperature values must also play an important role in determining the characteristics of the simulated fields. For example, if the temperature at the surface is lowered, then the inversion strength at that location should increase. The choice of surface temperatures used for these tests was based on observations taken on JD 278 and subsequently adjusted somewhat to provide better agreement with observed slope flow characteristics. The same surface temperatures were used in Test 1 and Test 2; for Test 3, the ambient profile of Test 1 was used while the temperature differences between the surface and the ambient atmosphere in Test 2 were used to specify new surface temperatures

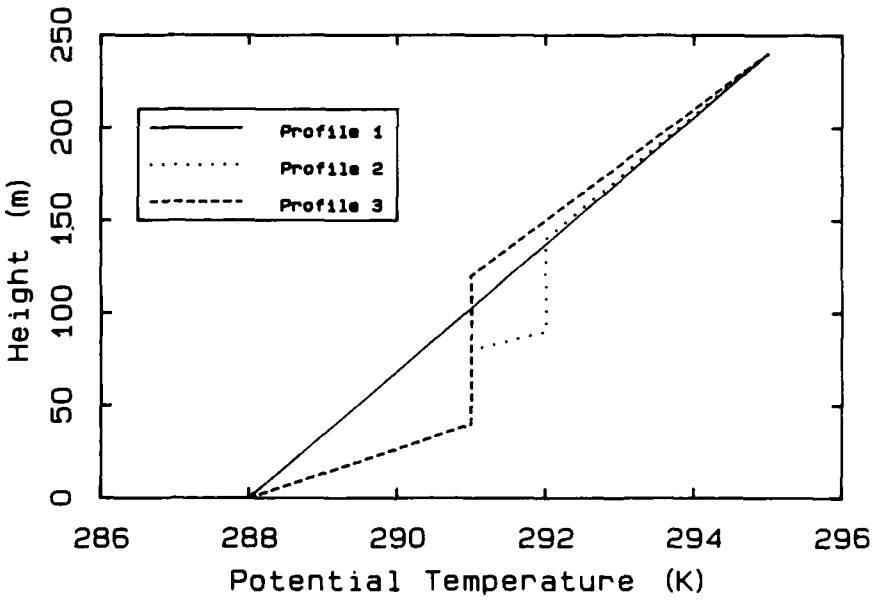

FIGURE 32. Potential Temperature Profiles Used for Simulations of Slope Flows Summarized in Table 6.

that maintained these differences. The results are given in Table 6, and show that the behavior of h does not correspond to observations.

TABLE 6. Results of Numerical Simulations for Various Combinations of Ambient Temperature Profiles, and Surface Temperatures

Test	h_A(m)	h_B(m)	h_C(m)	ΔT_A(K)	ΔT_B(K)	ΔT_C(K)
1	1.6	2.1	3.6	-1.6	-0.8	-0.4
2	1.8	1.2	1.2	-1.6	-1.5	-1.1
3	1.6	1.5	2.0	-1.7	-1.8	-1.0
4	1.8	1.7	1.2	-1.3	-0.7	-1.2
5	1.6	1.4	1.4	-1.7	-1.5	-1.1
6	1.2	0.9	0.8	-1.7	-1.6	-1.1

Test 1: Profile 1, Figure 32
Test 2: Profile 2, Figure 32
Test 3: As in Test 1, but with adjusted surface temperatures
Test 4: Profile 3, Figure 32
Test 5: As in Test 4, but with adjusted surface temperatures
Test 6: As in Test 2, but with reduced along-valley winds

We also tried a single region of constant potential temperature, as shown in Profile 3 in Figure 32. Our original surface temperature values yield the results summarized as Test 4 in Table 6; the results again do not agree with observations. When the surface temperatures were adjusted to yield the same differences between ambient and surface temperatures as found in Test 2, the development of h and ΔT with downslope distance agreed much better with observations (Test 5). Thus, there seem to be two requirements for reproducing the observed behavior of h and ΔT, the existence of regions of constant potential temperature and the proper choice of the surface temperatures for the lower boundary condition.

We remarked earlier that the behavior of the slope flows on the morning of JD 281 was atypical. Recall that the valley potential temperature profile on that morning had no region of constant potential temperature. Instead, there was an intense ground-based inversion, and the atmosphere became progressively less stable with height. During that period, the inversion depth measured at tower C was larger than at towers A or B; this was found on several mornings in the hours shortly before sunrise. This behavior is consistent with the results of our test simulations, which show that decreases in h with downslope distance seem to require the existence of some adiabatic layer in the ambient atmosphere.

Instead of specifying a surface temperature, sensible heat flux could have been specified along the lower boundary. However, there was no *a priori* information on the variation of the sensible heat flux with downslope distance, and when a constant value was assumed the results were not realistic. Moreover, the values of temperature used as a lower boundary condition were also used to calculate sensible heat fluxes using similarity theory. These results suggested that the heat flux was not constant down the slope, varying irregularly by a factor of three between towers A and C, and dropping to very small values below tower C. This drop may be related to the previously discussed problems with boundary conditions at the downslope edge of the model, but we are unable to test this. Observations also show that the use of a temperature difference between the surface and the ambient air that is independent of downslope distance, as assumed by Nappo and Rao (1987) and used in our first series of tests described previously, is also unrealistic. An example of this was given in Figure 20, which showed the inversion strength varying from tower to tower. A terrain-following three-dimensional model, with a rather complete surface energy budget to determine the proper lower boundary condition, seems required to address this feature of the simulation.

Another feature of slope flows shown by the model is that their development with downslope distance is not as regular as one might conclude from simply examining the results listed in Table 4. For example, in Test 2 described above,

h is equal to 1.2 m at towers B and C, but just below tower B the model showed h to be greater than 3 m. This region in the model was characterized by a very sharp increase in potential temperature between 80 and 90 m above the valley floor (Profile 2 in Figure 32). When a different profile was used, without this region of sharp increase in potential temperature (Profile 3 in Figure 32), the large jump in the value of h disappeared. This behavior again shows the sensitivity of the model to the details of the ambient temperature field. If the actual slope flows are similarly sensitive, then variations from the behavior summarized in the last column of Table 4 should not be uncommon. An example is given in Figure 33, which shows the variation of h at towers A, B, and C on the night of JD 278-279. For most of the night the behavior is similar to that previously shown in Figure 24 for JD 277-2788. However, there is a period of several hours before sunrise when the usual pattern is disrupted.

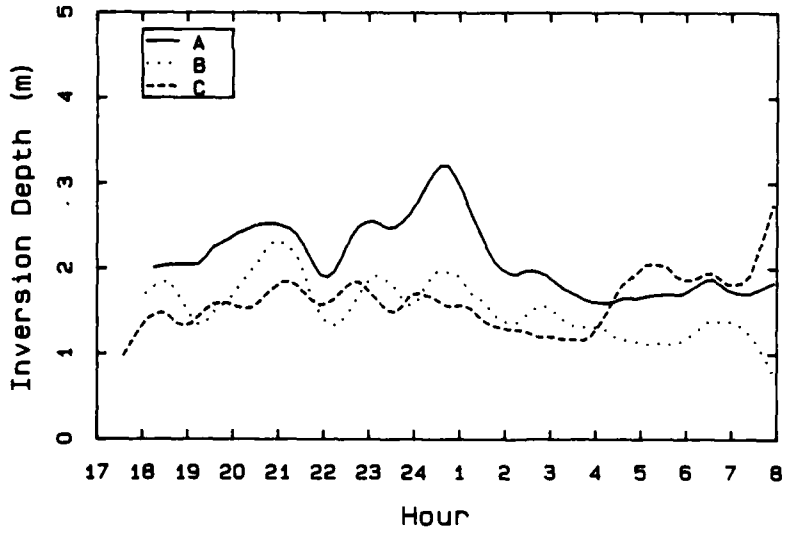

FIGURE 33. Inversion Depths at Towers A, B, and C on Night of JD 278-279.

The down-valley wind was also expected to have a significant influence on the slope flow characteristics, but the effects are more difficult to test with the model. It was noted earlier that once the down-valley winds increase, the local inversion strengths on the sidewall drop below their maximum values attained during the transition period. This effect was attributed to enhanced vertical mixing on the sidewalls. The model cannot properly simulate this physical mechanism without recourse to the use of a surface energy budget to determine the temperature or the sensible heat flux at the lower boundary. The ambient wind in the model can be reduced, but if the surface temperatures are not affected, the inversion strength is unlikely to change significantly. This is shown in Test 6 in Table 6. For this test, the ambient winds were reduced to 25% of the values used in the earlier tests. This results in reduced values of h because the mechanically generated TKE is less and vertical mixing is suppressed. This result is consistent with, but does not prove, our assertion that the development of the down-valley winds is instrumental in reducing the sidewall inversion strengths from their values realized during the evening transition period.

Finally, Figure 34 shows plots of the simulated wind and temperature fields at the positions of towers A, B, and C for the conditions used in Test 2. There is a slight strengthening of the katabatic winds between towers A and B, with a subsequent decrease at tower C. The maximum strengths of the winds compare well with observations but seem to fall off somewhat too rapidly with height. This could be caused by the neglect of ambient cross-valley winds that may be present. The inversion depth clearly decreases below tower A, and the inversion strength is noticeably smaller at tower C.

Although in Test 2 the inversion depth h decreased from tower A to C, the momentum depth h' increased by almost a factor of two. Thus, while the surface inversion became concentrated in a smaller depth (smaller h), the katabatic winds extended over a deeper layer (larger h'). This is a significant difference from the results over a simple slope with constant ambient stratification, where the two scales were closely related (Horst and Doran 1986). It is not surprising, then,

that the model predictions of Table 4 and the observations over valley sidewalls do not agree. However, it is not apparent how one would measure a momentum depth scale in the presence of cross-valley ambient winds.

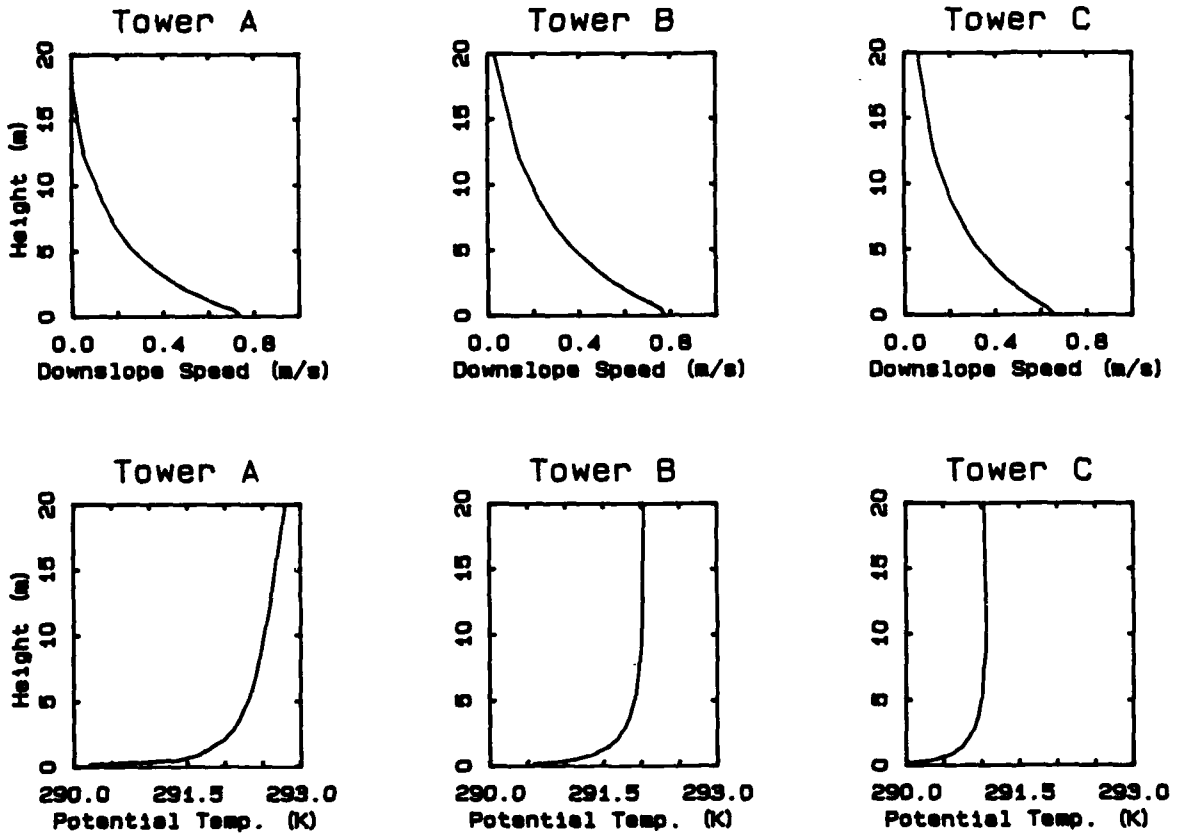

FIGURE 34. Simulated Wind and Temperature Profiles at Towers A, B, and C for Test 2.

SUMMARY AND CONCLUSIONS

Perhaps the clearest impression produced by this study of slope flows in a simple valley is that that their behavior is quite complex and not easily predicted by a few simple parameters. The development of katabatic flows on a valley sidewall was not readily inferred from studies of such flows on simple, isolated slopes, although such studies were quite useful in providing estimates of the relevant wind and temperature scales.

The detailed temperature structure of katabatic flows on valley sidewalls was found to be quite sensitive to the structure of the ambient temperature profile in the valley. However, the presence of cross-valley temperature gradients made it virtually impossible to define unambiguously an appropriate ambient profile based on measurements in the valley center. It is possible to characterize the temperature structure of slope flows in terms of two parameters, an inversion strength ΔT and an e-folding inversion depth h. After an initial transition period shortly after local sunset, the inversion depth on the east sidewall reaches a value on the order of 3 m in the upper third of the valley slope, and about 2 m in the lower half. These values usually decrease by about 1 m during the course of the night, with occasional increases of about 0.5 m in the lower third of the valley a few hours before sunrise. The inversion strength along the upper half of the slope typically peaks at values between 3 and 4 K during the transition period, and decreases to a value about one third as large later in the night. In the lower third of the valley, the inversion strength generally reaches a smaller peak value of about 1.4 K, which subsequently decreases to around 0.8 K. On the west sidewall, which goes into shadow earlier than the east sidewall, and which is covered with considerably thicker vegetation, the initial inversion strengths are several degrees larger than on the east sidewall. Their final values are not easily characterized and appear to depend on local topographical features, which are much more irregular on the west sidewall.

Katabatically induced slope winds are generally weak, with measured peak values less than 1 m/s for most of the night. Flows on the east sidewall average several tens of cm/s larger than those on the west wall. Observations and numerical simulations suggest that katabatic slope winds in this valley extend 10 m or more above the surface.

The ambient temperature profile in the valley frequently showed extended layers in which adiabatic conditions prevailed. Observations and numerical simulations show that these layers are associated with decreases in the slope flow inversion depth scale h, but the numerical simulations also showed that this does not necessarily imply a decrease in the momentum depth scale, h'. The latter scale is difficult to define or measure in the presence of ambient winds; in contrast, the inversion depth scale is better defined and its behavior can be described. Over simple slopes, the two depth scales will generally evolve similarly with downslope distance, but in a valley this need not be true.

Observations of the behavior of the net radiation (see Appendix A) and the timing of the formation of local inversions on the slopes imply that sky view factors are important in determining radiation budgets. The model results also suggest that a proper description of the valley flow dynamics requires a detailed surface energy budget description to properly determine the lower boundary condition for the thermodynamic equation. If the radiation contributions to this budget are to be handled correctly, then the effects of sky view factors should be included in the model. Moreover, assumptions of constant cooling rates, constant temperature deficits, or sensible heat fluxes independent of downslope position are not supported by this study.

The role of the along-valley wind is also an important one. When the down-valley winds are weak, the buoyancy deficit on the slopes can be large, and katabatic winds increase with increasing values of $h \cdot \Delta T$. However, the development of strong down-valley flows produces enhanced mixing along the slopes, which limits the strength of the inversion that can develop there. Near the valley floor, it

can prevent a strong local inversion from ever forming on the sidewall. Along the higher elevation slopes, the strength of the inversion that forms shortly after local sunset is subsequently reduced when the valley wind speeds increase. When the local sidewall inversions are only on the order of 1 to 2 K, the katabatic flows are weak, and the wind direction along the slopes is predominantly down-valley with a relatively small downslope component. Thus, the effects of the along-valley wind were at least as important as the valley inversion structure in determining the general features of katabatic flows on the slopes of a valley.

These conclusions suggest that the study of a trapping or weakly-draining valley or basin would be particularly interesting and important. In such a situation the development of the valley inversion would be far more critical in determining the flows along the slope, and the slope flows would be more likely to respond in the way originally envisioned and described in the introduction. Slope flows would be progressively cut off only as the valley inversion deepened, rather than by mixing processes induced by along-valley winds. Implications for air pollution, visibility, etc. are much more serious in such cases than in a valley that is well drained. It might also be easier to describe the evolution and characteristics of the slope flows in such a case, because the complication arising from the along-valley winds would be absent.

PUBLICATIONS AND PERSONNEL

"Wind and Temperature Structure on the Slopes of a Mountain Valley," by J.C. Doran, T.W. Horst and C.D. Whiteman was presented at the Fourth Conference on Mountain Meteorology, August 25-28, 1987, in Seattle, Washington, and appeared in the conference preprints.

During the course of this work, J.C. Doran, T.W. Horst, and C.D. Whiteman were the principal scientific personnel supported by project funds. Technical support was provided by O. B. Abbey, G. W. Dennis, J. M. Hubbe, J. Buck, D. Dovey and M. Schmeeckle.

LITERATURE CITED

Filliger, P., B. Rickli, and H. Wanner. 1987. Slope and Valley Wind Measurements and Their Comparison with Ambient Winds and Stability. In Preprints from the Fourth Conference on Mountain Meteorology, August 25-28, 1987, Seattle, Washington. American Meteorological Society, Boston, Massachusetts, pp. 70-75.

Horst, T.W., and J.C. Doran. 1986. Nocturnal Drainage Flow on Simple Slopes. Bound.-Layer Meteor. **34**, 263-286.

Manins, P.C., and B.L. Sawford. 1979. A Model of Katabatic Winds. J. Atmos. Sci. **36**, 619-630.

Mellor, G.L., and T. Yamada. 1982. Development of a Turbulence Closure Model for Geophysical Fluid Problems. Rev. Geophys. Space Phys. **20**, 851-875.

Nappo, C.J., and K.S. Rao. 1987. A Model Study of Pure Katabatic Flows. Tellus **39A**, 61-71.

Prandtl, L. 1942. Strömungslehre [Flow Studies]. Vieweg und Sohn, Braunschweig, 382 pp.

Whiteman, C. D. 1986. "Temperature Inversion Buildup in Colorado's Eagle Valley." Meteor. Atmos. Phys. **35**, 220-226.

APPENDIX A

ENERGY BUDGETS

APPENDIX A

ENERGY BUDGETS

Original field plans were to measure radiation and surface energy budget components with the Bowen ratio energy budget technique. These plans were abandoned, however, after problems were encountered with this technique in a previous experiment measuring small nighttime values of fluxes. Net radiation measurements at five of the tower sites were substituted for the planned surface energy budget measurements. It was hoped that these measurements would be sufficient to enable us to estimate nighttime sensible heat fluxes. These downward heat fluxes from the atmosphere to the surface cool a shallow layer of air above the slope. Negative buoyancy forces in this layer lead to the katabatic winds. In the following section we attempt to estimate surface sensible heat fluxes in the valley. These are then used to investigate the rate of cooling of the entire valley atmosphere on a vertical valley cross section. The along-valley circulations in a valley are driven by pressure gradients that are built up hydrostatically along a valley's length due to differential cooling along a valley's length. The cooling in a valley cross section is therefore a key determinant of the strength of the along-valley wind system in a given valley.

NET RADIATION

Net all-wave radiation is presented in Figure A.1 as a function of time for five of the tower sites in the Touchet Valley. We will concentrate attention on the nighttime period of JD 278, a typical period with respect to net radiation. The sudden afternoon drop in net radiation at sites E and F indicates the times of local sunset. There is little variation in net radiative loss from site to site on a given sidewall. Average nighttime net radiative losses at the west sidewall sites (34 W/m^2) are lower than corresponding losses from the east sidewall sites (45 W/m^2). On JD 278 the nighttime net radiative loss was constant during most of the night.

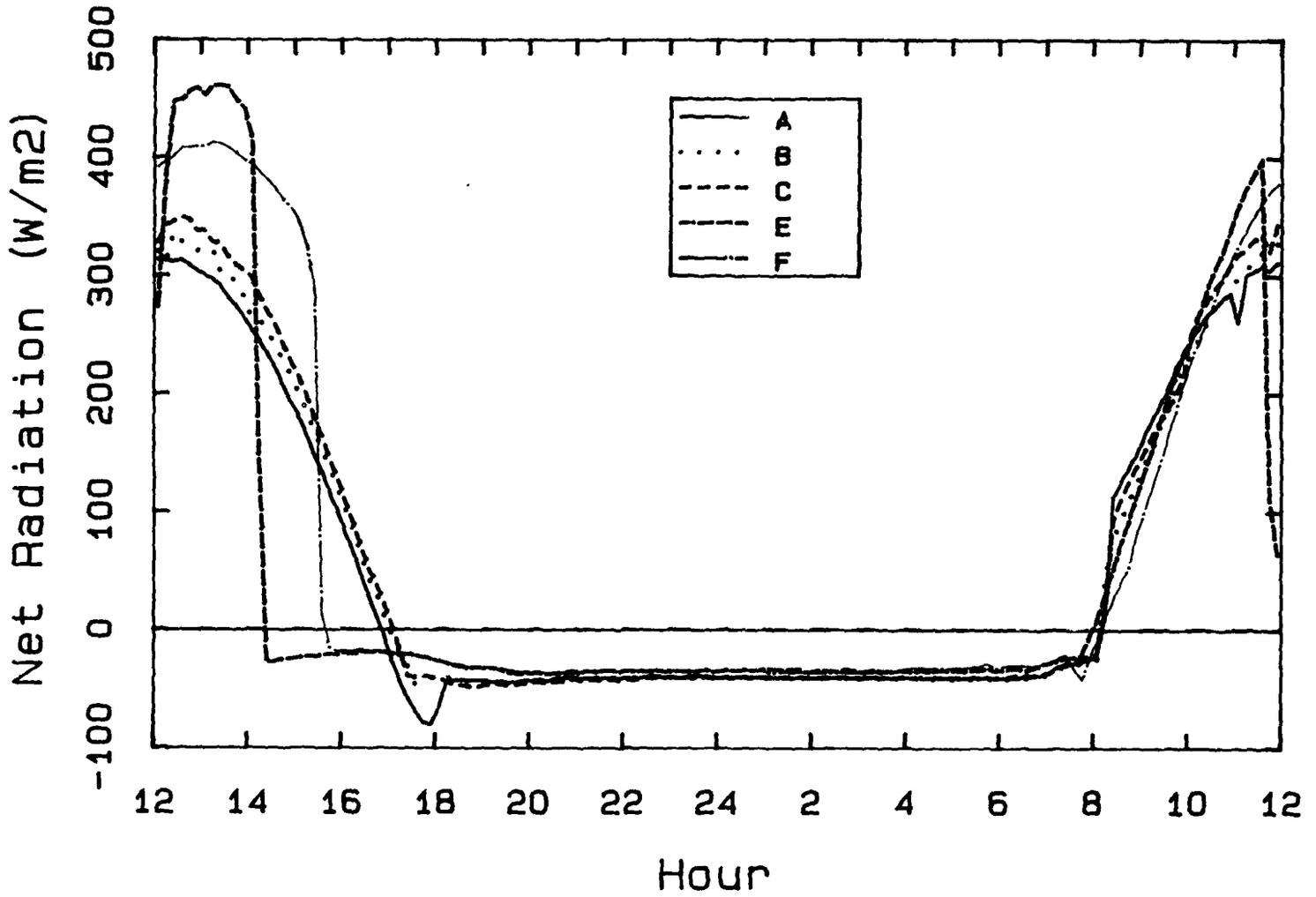

FIGURE A.1. Net Radiation at Five Tower Locations Versus Time, S. Fork Touchet Valley, Julian Date 277-278.

On several other clear nights, however, the net radiative loss decreased slowly through the night from 50 W/m^2 to 40 W/m^2.

As previously mentioned, the east sidewall towers were shaded in the order C, B, A. Despite this sequence of shading, the sign reversal of net radiation occurred first at tower A, then at tower B and finally at tower C. The times of sign reversal for towers A, B, and C on Day 277-278 were, respectively, 1656, 1705, and 1712 PDT. The sign change at A occurs about 1 hour and 6 min before sunset, at B about 35 min before sunset, and at C several minutes before sunset. This timing is inferred to be caused primarily by the altitudinal variation of downward longwave radiation in the valley. This can be illustrated with the radiation budget equation

$$Q^* = K_{up} + K_{dn} + L_{up} + L_{dn} \qquad [W/m^2] \qquad (A.1)$$

where Q^* is net all-wave radiation, K_{up} and K_{dn} are the fluxes of incoming and reflected short wave radiation and L_{up} and L_{dn} are the fluxes of upward- and downward-directed long wave radiation. K_{dn} and K_{up} suddenly become quite small when shading occurs at an observing site, as the only contribution to K_{dn} then comes from sky radiation and the radiation reflected from surrounding terrain. From the Stefan-Boltzmann law, L_{up} depends on the ground temperature. L_{dn}, on the other hand, varies with elevation on the sidewall because of the varying sky view factor. The uppermost site has a nearly unobstructed view of the cold radiating sky hemisphere. Sites farther down the sidewall, however, see a hemisphere that contains partly sky and partly warm radiating sidewalls. Thus L_{dn} decreases with elevation. This decreased longwave radiation is apparently sufficient to reverse the radiation budget earlier on the upper sidewall than on the lower sidewall, despite the counteracting influence of the shortwave radiative terms.

SURFACE ENERGY BALANCE

The surface energy balance is expressed as

$$Q^* + Q_G + Q_H + Q_E = 0 \quad [W/m^2] \qquad (A.2)$$

where Q_G is the ground heat flux, Q_H is the surface sensible heat flux, Q_E is the latent heat flux, and the sign convention is that all heat fluxes toward the surface, whether from the atmosphere or the ground, are positive. From measurements of net radiation we attempt in this section to estimate the surface sensible heat flux.

Average nighttime net radiative losses from the valley's east sidewall were about 45 W/m^2. Losses were 5 to 10 W/m^2 less on the west sidewall. Considering both sidewalls, the net radiative loss from the valley cross section would be near 40 W/m^2 (i.e., $Q^* = -40$ W/m^2).

The longwave loss is typically counteracted by an upward flux of heat towards the surface from the soil. For illustration, we will assume a ground heat flux Q_G of +15 W/m^2, which is close to values obtained in a previous experiment in Colorado. From Equation (A.2), we may then solve for the sensible heat flux

$$Q_H = -(Q^* + Q_G) - Q_E = 25 - Q_E \quad [W/m^2] \qquad (A.3)$$

If we assume that the latent heat flux is negligible, sensible heat flux may be estimated as $Q_H = 25$ W/m^2. Following our sign convention, this represents a flux of heat from the atmosphere to the surface, resulting in cooling of the atmosphere. If the normal daytime evaporation continues into the night, Q_E will be negative (the surface loses energy) and sensible heat flux towards the surface will be correspondingly increased. If dew is deposited on the surface, Q_E will be positive and sensible heat flux will be correspondingly smaller than 25 W/m^2. Typical latent heat fluxes on dewfall nights are expected to be small, perhaps in the range of 5 to

10 W/m² (Monteith 1957), so that we may estimate sensible heat flux on nights with dewfall to be perhaps 15 to 20 W/m². On non-dewfall nights sensible heat flux is expected to be 25 W/m² or more. Qualitative dewfall observations were made at the tethered balloon site on all experimental nights. On JD 276 and 277 dewfall was light to moderate, on JD 278, 279 and 280 dewfall was light, and on JD 281 dewfall was moderate to heavy. Humidities are presumed to be higher at the tethered balloon site (center of valley floor near the river) than on the dry sidewalls. In fact, the limited number of nighttime observations on the sidewalls indicated no dew formation whatever. If we assume that dew formation occurred only on the valley floor, we may estimate the nighttime sensible heat fluxes on the entire valley cross section as being near the 25 W/m² value that would be attained with negligible latent heat flux.

ATMOSPHERIC ENERGY BUDGET

The atmospheric energy budget for a valley volume may be written as

$$\iiint \left\{ \rho c_p \frac{\partial \bar{\theta}}{\partial t} = -\rho c_p \mathbf{V} \cdot \nabla \bar{\theta} - \nabla \cdot \mathbf{H} - \nabla \cdot \mathbf{R} \right\} dV \quad [W] \qquad (A.4)$$

where **V** is the vector wind, **H** is the vector turbulent sensible heat flux, **R** is the vector net radiation, V is the atmospheric volume, and other symbols take their usual meaning. The integration is performed for a unit-deep vertical cross section of the valley to ridgetop height z = h, where W(z) is the valley width. The local rate of change of mean potential temperature is assumed to be independent of cross-valley distance y, Green's Theorem is used to simplify the integration of the radiative and sensible heat flux divergences, and all terms in the equation are divided by the area W(h) at the top of the unit-deep cross section so that each term in the equation has the units of energy flux density [W/m²]. We thus obtain the equation

$$\frac{\int_0^h \rho c_p \frac{\partial \bar{\theta}}{\partial t} W(z)\, dz = -\iiint \rho c_p \mathbf{V} \cdot \nabla \bar{\theta}\, dV - \iint \mathbf{H} \cdot d\mathbf{S} - \iint \mathbf{R} \cdot d\mathbf{S}}{W(h)} \quad [W/m^2] \qquad (A.5)$$

The radiative flux divergence term (i.e., the last term in the equation) has been evaluated by other investigators with radiative transfer models (Freytag 1985; Horst et al. 1987). These evaluations have been somewhat unsatisfactory due to the usual practice of using a plane parallel (i.e., horizontally homogeneous) model atmosphere. All investigators appear to agree, however, that the magnitude of this term during nighttime is small. For the present purposes radiative flux divergence is expected to produce a nighttime loss of 10 W/m^2 or less, in keeping with previous estimates. Further work seems advisable, however, to estimate this term better.

The sensible heat flux divergence term (next to last term in Equation (A.5)) is composed of three components. The two horizontal sensible heat flux divergence components are assumed negligible compared to the vertical sensible heat flux divergence. The vertical sensible heat flux divergence is then evaluated by summing the fluxes coming across the surfaces that enclose the valley cross section. The flux across the top of the valley atmosphere through area W(h) is presumed small compared to the surface fluxes, in agreement with Hacker's (1982) motorglider measurements above the Dischma Valley. This is in accordance with our expectations that vertical turbulent sensible heat flux divergence occurs in a shallow layer above the surfaces during stable conditions, so that vertical gradients of sensible heat flux decrease higher in the atmosphere. Nighttime surface turbulent sensible heat flux H(0) in the Touchet valley is estimated at 25 W/m^2 (see paragraph on surface energy budget above). The heat flux out of the atmospheric volume at the surfaces would then be given by the product of this flux and the area through which it acts, which is the ridge to ridge distance as measured along the ground, L. This distance is only about 10% greater than W(h), so that the the sensible heat flux term reduces to

$$\frac{\iint \mathbf{H} \cdot d\mathbf{S}}{W(h)} = \frac{25\,L}{W(h)} \cong 25 \quad [W/m^2] \qquad (A.6)$$

Thus, nighttime turbulent sensible heat flux divergence is expected to produce a loss of energy from the valley atmosphere at the rate of 25 W/m^2.

The term on the left of Equation (A.5) represents the rate of change of heat storage in the cross section. It has been calculated for the Touchet Valley from consecutive tethered balloon potential temperature soundings and is plotted in Figure A.2 for JD 277, 278, and 281. From this figure we see that the rate of decrease of energy storage in the valley cross section is less than or approximately equal to the 35 W/m^2 heat loss from the local diabatic terms (sensible heat flux divergence plus radiative flux divergence) before 1730 PDT. There is some indication, as well, of energy storage changes at this rate after 1930 PDT. During these times the rate of change of energy storage in the valley can be easily accounted for by the two diabatic processes. Between these periods, however, advection (the remaining un-evaluated term in Equation (A.3) appears to be necessary to account for the observed loss of heat from the cross section, which on all three nights attains values in excess of 70 W/m^2. Thus, we must conclude that cold air advection (either along-valley advection, upward vertical motion, or both) plays an important role in the cooling of the valley cross section during the evening transition period during the time period from 1730 to 1930 PDT.

In the Touchet Valley, the cooling of the cross section under investigation has a strong advective component -- at least during a brief time in the evening transition period. The significance of this is clear. Modeling efforts to explain the development of along-valley circulations in this valley will have to be fully three-dimensional, because local diabatic processes are not fully responsible for the observed cooling.

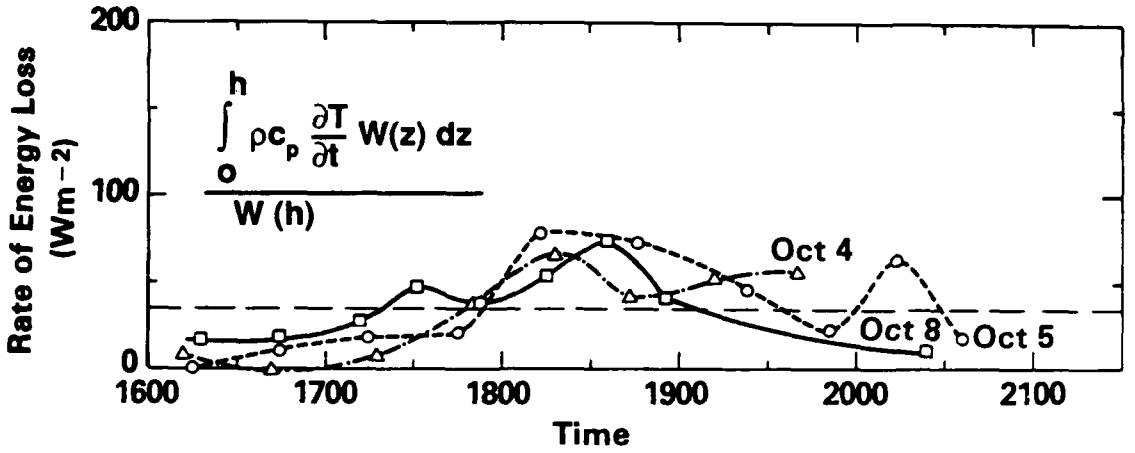

FIGURE A-2. Rate of Loss of Heat From a Unit-Thickness Valley Cross Section as a Function of Time During the Evening Transition Period, S. Fork Touchet Valley, Julian Dates 277, 278, and 281. The estimated value of the sum of the radiative flux divergence and sensible heat flux divergence is indicated by the horizontal dashed line at 35 W/m^2.

LITERATURE CITED

Freytag, C. 1985. MERKUR-Results: Aspects of the Temperature Field and the Energy Budget in a Large Alpine Valley During Mountain and Valley Wind. Contrib. Atmos. Phys. **58**, 458-476.

Hacker, J.M. 1982. Preliminary Results of the Alpine Experiment DISKUS. Aero Review **10**, 44-49.

Horst, T.W., K.J. Allwine, and C.D. Whiteman. 1987. "A Thermal Energy Budget for Nocturnal Drainage Flow in a Simple Valley." In Preprints from the Fourth Conference on Mountain Meteorology, August 25-28, 1987, Seattle, Washington. American Meteorological Society, Boston, Massachusetts, pp. 15-19.

Monteith, J. L. 1957. "Dew." Quart. J. Roy. Meteor. Soc. **83**, 322-341.

APPENDIX B

MODEL EQUATIONS

APPENDIX B

MODEL EQUATIONS

The equation for the downslope wind component u is

$$\frac{\partial u}{\partial t} = -u\frac{\partial u}{\partial s} - w\frac{\partial u}{\partial n} - g\frac{\theta'}{\theta_o}\sin\beta + \frac{\partial}{\partial n}\left(K_m\frac{\partial u}{\partial n}\right) + \frac{g}{\theta_o}\cos\beta\frac{\partial}{\partial s}\left(\int_n^{h_r}\theta' dn\right) \qquad (B.1)$$

where w is the wind component normal to the slope, β is the slope angle, K_m is a turbulent exchange coefficient for momentum, θ_0 is the ambient potential temperature, $\theta' = \theta'(n)$ is the deviation from the ambient potential temperature arising from the cooling of the surface at the sidewalls, and h_r is a height where θ' goes to zero. This equation is the same as that used by Nappo and Rao (1987) in their model.

The continuity and thermodynamic equations are given by

$$\frac{\partial u}{\partial s} + \frac{\partial w}{\partial n} = 0 \qquad (B.2)$$

and

$$\frac{\partial \theta}{\partial t} = -u\frac{\partial \theta}{\partial s} - w\frac{\partial \theta}{\partial n} + \frac{\partial}{\partial n}\left(K_h\frac{\partial \theta}{\partial n}\right) \qquad (B.3)$$

where K_h is a turbulent exchange coefficient for heat.

The turbulent kinetic energy (TKE) e is computed from

$$\frac{\partial e}{\partial t} = - u\frac{\partial e}{\partial s} - w\frac{\partial e}{\partial n} + K_m\left\{\left(\frac{\partial u}{\partial n}\right)^2 + \left(\frac{\partial v}{\partial n}\right)^2\right\} + \frac{\partial}{\partial n}\left(K_e\frac{\partial e}{\partial n}\right)$$

$$- \frac{g}{\theta}K_h\frac{\partial \theta}{\partial n}\cos\beta[F] - 2^{\frac{3}{2}}\frac{c_\epsilon e^{\frac{3}{2}}}{l} \qquad \text{(B.4)}$$

where the usual buoyancy production term is modified by a factor F. This factor arises from the effects of the horizontal (slope parallel) heat flux (Horst and Doran 1988) and is a function of the local shear and the ratio of the horizontal to normal heat fluxes. For our simulations F usually did not differ significantly from a value of 1. In Equation (B.4), K_e is an exchange coefficient for TKE, c_ϵ is a constant equal to 0.139, and l is a mixing length given by

$$\frac{1}{l} = \frac{1}{kn} + \frac{1}{l_0} \qquad \text{(B.5)}$$

The coefficient k is von Karman's constant and l_0 is a limiting mixing length given by

$$l_0 = 0.10\frac{\int_0^\infty qn\,dn}{\int_0^\infty q\,dn} \qquad \text{(B.6)}$$

where q^2 is twice the TKE (Mellor and Yamada 1982).

Nieuwstadt (1984) and Horst and Doran (1988) used a different expression for the mixing length in their analyses of stably stratified flows. The expression above gave larger exchange coefficients and improved the performance of the model when compared to observations.

The equation for the TKE also contains the cross-slope (down-valley) wind component v, which is calculated from

$$\frac{\partial v}{\partial t} = \frac{\partial}{\partial n}\left(K_m \frac{\partial v}{\partial n}\right) \qquad \text{(B.7)}$$

Cross-slope winds at the top of the model domain were assumed equal to the observed along-valley winds in the center of the valley at the corresponding heights. The vertical distribution of v in the model domain was then found from the above equation.

MODEL DOMAIN

The model domain was a grid with 13 points in the horizontal and 15 in the vertical. A staggered grid was used in which θ, e, and w were offset by one half of a grid increment in the horizontal from the velocity components u and v. The horizontal spacing was 50 m. The spacing for the (e,w) grid points varied from 0.30 m near the surface to 40 m at the top of the domain (100 m). The quantities u,v and θ were defined at points midway between the (e,w) grid points.

One external grid point was defined at the top of the model, and e was set equal to a background value of 10^{-4} m^2/s^2 there. In Equation (B.6) , this marked the actual upper limit of integration in the calculation of l_0.

LITERATURE CITED

Horst, T.W., and J.C. Doran. 1988. The Turbulence Structure of Nocturnal Slope Flow. J. Atmos. Sci. **45**, 605-616.

Mellor, G.L., and T. Yamada. 1982. Development of a Turbulence Closure Model for Geophysical Fluid Problems. Rev. Geophys. Space Phys. **20**, 851-875.

Nappo, C.J., and K.S. Rao. 1987. A Model Study of Pure Katabatic Flows. Tellus **39A**, 61-71.

Nieuwstadt, F.T.M. 1984. The Turbulence Structure of the Stable, Nocturnal Boundary Layer. J. Atmos. Sci. **41**, 2202-2216.